Journal of Geophysical Research: Earth Surface

RESEARCH ARTICLE
10.1029/2018JF004612

Unifying Particle-Based and Continuum Models of Hillslope Evolution With a Probabilistic Scaling Technique

J. Calvert[1], **M. Balázs**[2], **and K. Michaelides**[3,4]

[1]Department of Statistics, University of California, Berkeley, Berkeley, CA, USA, [2]School of Mathematics, University of Bristol, University Walk, Bristol, UK, [3]School of Geographical Sciences, University of Bristol, Bristol, UK, [4]Earth Research Institute, University of California, Santa Barbara, CA, USA

Key Points:
- We present a particle-based model of hillslope evolution
- Probabilistic scaling of the particle model gives a continuum advection-diffusion equation
- The scaling argument bridges the microscopic and macroscopic descriptions of the hillslope evolution model

Correspondence to:
J. Calvert,
jacob_calvert@berkeley.edu

Citation:
Calvert, J., Balázs, M., & Michaelides, K. (2018). Unifying particle-based and continuum models of hillslope evolution with a probabilistic scaling technique. *Journal of Geophysical Research: Earth Surface, 123*. https://doi.org/10.1029/2018JF004612

Received 9 JAN 2018
Accepted 19 OCT 2018
Accepted article online 29 OCT 2018

Abstract Relationships between sediment flux and geomorphic processes are combined with statements of mass conservation, in order to create continuum models of hillslope evolution. These models have parameters that can be calibrated using available topographical data. This contrasts the use of particle-based models, which may be more difficult to calibrate but are simpler and easier to implement and have the potential to provide insight into the statistics of grain motion. The realms of individual particles and the continuum, while disparate in geomorphological modeling, can be connected using scaling techniques commonly employed in probability theory. Here we motivate the choice of a particle-based model of hillslope evolution, whose stationary distributions we characterize. We then provide a heuristic scaling argument, which identifies a candidate for their continuum limit. By simulating instances of the particle model, we obtain equilibrium hillslope profiles and probe their response to perturbations. These results provide a proof of concept in the unification of microscopic and macroscopic descriptions of hillslope evolution through probabilistic techniques and simplify the study of hillslope response to external influences.

1. Introduction

Hillslopes evolve topographically through a variety of erosional mechanisms ranging from slow diffusive processes (e.g., soil creep), to fast, localized processes (e.g., landslides). Over short timescales ($10^0 - 10^1$ years), hillslope sediment transport determines the redistribution of sediment and its delivery to the slope base. Over long timescales ($10^2 - 10^5$ years) the balance between, and integral of, individual erosional events determines the topographic form of hillslopes. Where advective processes dominate, hillslopes tend to be concave up, and where diffusive processes are more pronounced hillslopes become convex (e.g., Carson & Kirkby, 1972; Kirkby, 1971). It is well acknowledged that the processes shaping landscapes are inherently dynamic and stochastic (Dietrich et al., 2003; Roering, 2004; Tucker & Hancock, 2010), yet landscape evolution model (LEM) characterization of hillslope processes is often based on geomorphic transport laws (GTLs), mathematical formulations expressing erosion as an averaged process operating over long timescales (Dietrich et al., 2003). This discrepancy gives rise to a mathematical disconnect between the stochastic processes operating at the grain scale over the short term and the evolution of hillslope topography over the long term.

In this paper we demonstrate a probabilistic scaling argument by which a particle-based description of hillslope sediment transport can be scaled to a continuum one representing long-term hillslope evolution. In other words, we present a mathematical argument for deriving a continuum description of hillslope erosion while remaining faithful to the particle-scale dynamics that operate over short temporal and spatial scales.

GTLs are a compromise between a comprehensive physics-based description, which may be too complex to be parametrized through field observation, and rules-based modeling, which may lack a testable mechanistic footing (Dietrich et al., 2003). LEMs typically consist of a statement of mass conservation, GTLs for describing sediment transport in the form of differential equations, and numerical methods to approximate solutions to the GTLs (Tucker & Hancock, 2010). Despite inherent simplifying assumptions associated with this approach, GTLs have been successful in simulating landform development in some environments, particularly associated with diffusive processes like creep and bioturbation (e.g., Roering et al., 1999).

Particle-based models, which display a rich range of behavior despite their simplicity and ease of implementation, are an important alternative to this prescription of landscape evolution modeling (Davies et al., 2011;

Kessler & Werner, 2003; Tucker & Bradley, 2010). Traditionally, particle models have been criticized for using *ad hoc* evolution rules and experimentally inaccessible parameters and for neglecting the underlying transport physics (Dietrich et al., 2003). Accordingly, as continuum models have long been numerically implementable and experimentally verifiable, the use of GTLs has dominated studies of landscape evolution. However, the experimental validation of particle-based models is now possible using techniques for tracking grain motion (Fathel et al., 2015; Habersack, 2001; McNamara & Borden, 2004; Roering, 2004; Roseberry et al., 2012). This, combined with their ability to incorporate particle mechanics and motion statistics, leads Tucker and Bradley (2010) to argue that particle-based models are no less fundamental than GTLs and should be used to complement continuum models.

While the case against the use of particle-based models has been undermined by experimental innovation, it is the theoretical development of nonlocal transport on hillslopes, which best underscores the case for their use. Continuum models like those of Culling (1963) and Andrews and Bucknam (1987) rely on locality assumptions, the assumption that sediment transport at position x on a slope is a function of the hillslope conditions at x (i.e., local land surface slope; Furbish, Haff, et al., 2013). Locality assumptions are only valid when hillslope material moves short distances relative to the hillslope length (Tucker & Bradley, 2010). Examples of local transport processes are soil creep (Furbish, Haff, et al., 2009), rainsplash (Dunne et al., 2010; Furbish, Childs, et al., 2009), and bioturbation and tree throw (Gabet, 2000; Gabet et al., 2003). Nonlocal transport occurs when sediment transport at position x depends on the hillslope characteristics a significant distance upslope or downslope of position x (Furbish, Haff, et al., 2013) such that occurs in sheetwash sediment transport (Michaelides & Martin, 2012; Michaelides & Singer, 2014) and dry ravel (Gabet & Mendoza, 2012) on steep slopes. Accordingly, formulations of nonlocal transport must specify the relationship between flux and relative upslope or downslope position, ultimately leading to assumptions on the distribution of particle travel distances (Furbish & Haff, 2010; Furbish, Haff, et al., 2013) or the fitting of a fractional derivative operator (Foufoula-Georgiou et al., 2010). However, such relationships change as hillslopes evolve, and so particle-based approaches may be more appropriate (DiBiase et al., 2017; Gabet & Mendoza, 2012).

In order to effectively combine their strengths, the particle model must correspond, in some sense, to the continuum description. However, as Tucker and Bradley (2010) indicate, it is not clear how to identify such a pair. Indeed, referring to the particle-based models of Tucker and Bradley (2010) and Gabet and Mendoza (2012), Ancey et al. (2015) observe, "there is no technique for deriving continuum equations from the rules used to describe particle behavior in this environment." Here we demonstrate a *probabilistic scaling* argument by which a particle-based description can be scaled to a continuum one with the two descriptions corresponding to one another. The probabilistic scaling procedure consists of scaling space and time by a small parameter, ultimately converting the microscopic evolution rules into a partial differential equation governing the macroscopic observables (Bahadoran et al., 2010; Kipnis & Landim, 1999; Olla et al., 1993).

In sections 2 and 3, we introduce a simple particle-based model of hillslope evolution and provide a heuristic scaling argument, which identifies a corresponding continuum description in the form of an advection-diffusion equation. Critically, the particles of our model correspond to characteristic units of hillslope *gradient*, not hillslope height. This element of indirection softens the distinction between local and nonlocal transport, and for this reason, our model can represent diverse geomorphic processes and the scaling argument applies uniformly across various transport regimes.

Finessing nonlocal transport through indirection comes at the expense of immediate access to information about particle hopping distances and fluxes. This contrasts the convolutional approaches of Foufoula-Georgiou et al. (2010) and Furbish and Haff (2010), which express sediment flux arising from nonlocal transport as an integral over relative upslope positions. While such methods enable detailed calculation of fluxes, they require as input assumptions about the distribution of particle hopping distances in relation to hillslope topography (Gabet & Mendoza, 2012; Furbish & Haff, 2010; Furbish, Haff, et al., 2013). When these detailed outputs are unnecessary, the requisite inputs are unavailable, or corresponding simulations are computationally expensive, a particle-based approach may be preferable.

Section 4 describes simulations of the particle model for various choices of microscopic parameters, including both linear and nonlinear slope dependence, to exhibit the types of hillslope profiles that form and how fluxes arise in response to hillslope perturbations. Additionally, to translate simulation results into empirically testable predictions, we suggest a way of fitting model parameters from data and assigning dimensions to

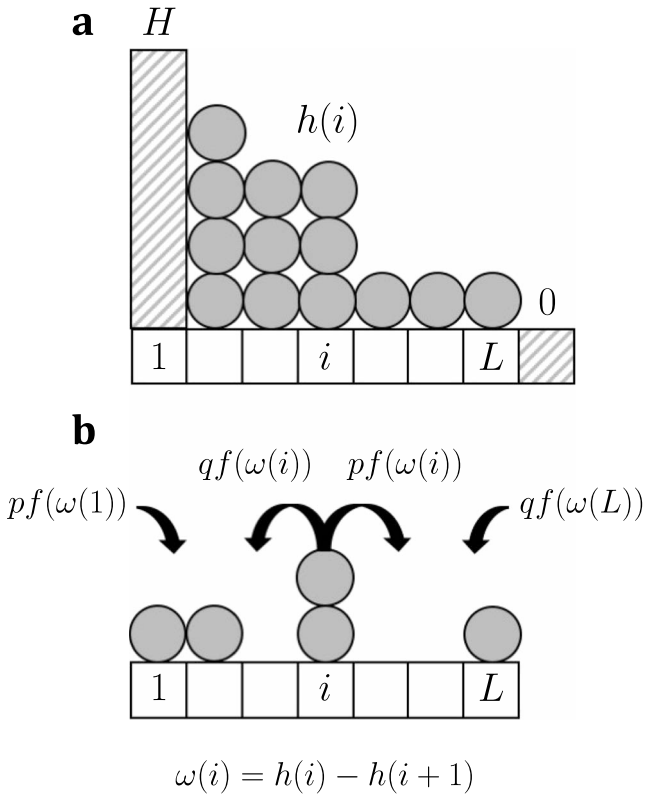

Figure 1. Schematic of the mapping between units of hillslope (a) and corresponding units of gradient (b). The height of the hillslope's leftmost site ($i = 1$) is fixed at a height of H and the rightmost site ($i = L + 1$) is fixed at 0 (a). In the gradient model (b), particles in the bulk ($1 < i < L$) hop to the left and right with rates $qf(\omega(i))$ and $pf(\omega(i))$, respectively; particles at the left boundary move right at rate $pf(\omega(1))$ and those at the right boundary move left at rate $qf(\omega(L))$.

model outputs. Finally, in section 5, we discuss the relation of this paper to the hillslope evolution and nonlocal transport literature and suggest future work, which takes advantage of a dual, particle-based and continuum approach.

2. A Particle-Based Model of Hillslope Evolution

2.1. Specifying State Space and Dynamics

As our goal is to model hillslope profiles, we begin by considering a 1-D grid of $L + 1$ labeled sites, each containing some number of *units* of hillslope height (Figure 1a). In other words, if a site contains two hillslope units, the hillslope has an elevation of twice some characteristic height. We fix the ridge-top height—the number of units at site 1—to be H and the number at site $L + 1$ to be 0. The process of hillslope evolution could then occur via the rearrangement of the units across sites 2 to L, according to some dynamics. In this case, the particles of an associated particle-based model would be identified with these units of hillslope height, like in the particle-based model of Tucker and Bradley (2010). However, our analysis becomes simpler if we instead specify the dynamics of a corresponding model, for which the particles are identified with units of hillslope gradient (Figure 1b). In other words, by each particle, we represent some characteristic difference in height over adjacent lattice sites. We will refer to these particles as gradient particles and the associated particle-based model as the gradient model, to distinguish them from particles representing units of hillslope height and the particle-based model that describes the evolution of the hillslope height profile.

If at time τ there are $h_\tau(i)$ units of hillslope height at site i and $h_\tau(i + 1)$ units of hillslope height at site $i + 1$, we place $\omega_\tau(i) = h_\tau(i) - h_\tau(i + 1)$ units of hillslope gradient at site i of the gradient model. We note that, because we fixed site $L + 1$ to have 0 units, $\omega_\tau(L) = h_\tau(L)$. Additionally, because we fixed site 1 to have H units, for any τ, it must be that $\sum_{i=1}^{L} \omega_\tau(i) = H$; we have conservation of gradient particles. To complete the specification of the gradient model, we need to describe the ways in which units of gradient—the particles of our gradient model—are allowed to move.

Figure 1 summarizes the rules governing the dynamics. Particles hop after exponentially distributed waiting times (a mathematical necessity), with rates given as follows. For sites $i \neq 1, L$, a particle will hop $i \to i + 1$ with rate $pf(\omega_\tau(i))$ and $i \to i - 1$ with rate $qf(\omega_\tau(i))$, where $p, q \in (0, 1)$ and $p + q = 1$, and $f(\omega_\tau(i))$ is a nondecreasing function of $\omega_\tau(i)$ with $f(0) = 0$. We note that the mean of an exponentially distributed time is the inverse of the hopping rate. The requirement that f be nondecreasing in $\omega_\tau(i)$ formalizes the intuition that the dynamics on steep slopes happen at least as quickly as those on gradual slopes. At the left boundary $i = 1$, a particle hops $1 \to 2$ with rate $pf(\omega_\tau(1))$ and, at the right boundary $i = L$, a particle hops $L \to L - 1$ with rate $qf(\omega_\tau(L))$. As the number of gradient particles $\omega_\tau(i)$ represents the steepness of the hillslope at site i, a gradient particle hopping to site i corresponds to the hillslope becoming steeper at i. This could reflect deposition at site i or erosion at site $i + 1$, both of which would cause the hillslope to become steeper at i (Figure 2). Specifically, if the gradient particle hops from site $i - 1$ to site i, it corresponds to deposition at site i for h_τ. Alternatively, if the gradient particle hops from site $i + 1$ to site i, it corresponds to erosion at site $i + 1$ for h_τ.

Particles in the gradient process only hop unit distances, unlike particles in the model of Tucker and Bradley (2010). However, while gradient particles redistribute locally, the corresponding changes in the height profile need not be. Consider again Figure 2—neither the origin of the deposited hillslope material nor the destination of the eroded hillslope material are specified. In other words, there is no conservation of units of hillslope. We discuss the consequences for fluxes in section 4.2.

Our model is a type of *continuous-time Markov process*, known in the statistical physics and probability literature as a *zero-range process* because particles hop at rates that depend on the occupancy of their current

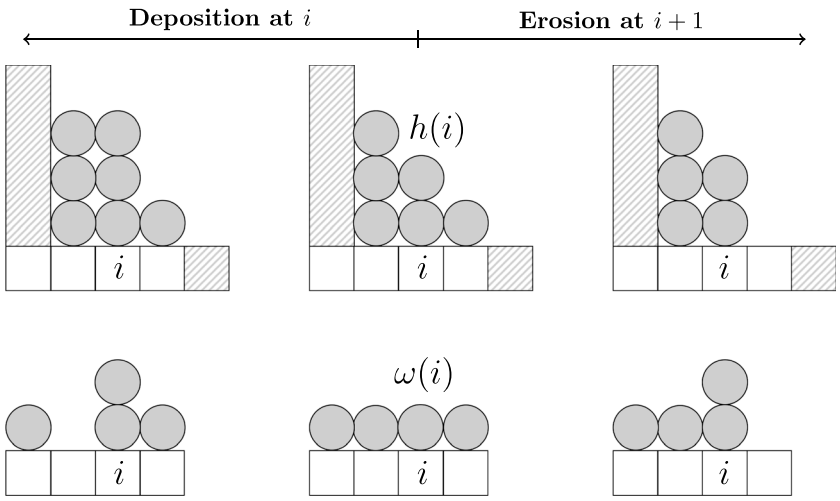

Figure 2. Deposition and erosion. Deposition at hillslope site i occurs when a gradient particle hops from site $i-1$ to site i (left). Erosion at hillslope site $i+1$ occurs when a gradient particle hops from site $i+1$ to site i (right). In both of the depicted cases, $\omega(i)$ increases, which is reflected in a steepening of $h(i)$ relative to $h(i+1)$. Analogously, there are deposition and erosion scenarios in which $\omega(i)$ decreases, corresponding to a lowering of $h(i)$ relative to $h(i+1)$.

site. In this sense, there is a zero-range interaction between particles occupying the same site. We note that exponentially distributed waiting times are characteristic of continuous-time Markov processes.

2.2. Identifying the Stationary Distributions of the Particle Model

2.2.1. The Detailed Balance Condition

The stationary distributions of the gradient process are those probability distributions over occupancies ω that are unchanged by the dynamics specified in section 2.1. In the context of our model, these stationary distributions represent the topographic steady state. The gradient process is in equilibrium when ω is distributed according to a stationary distribution. Denoted by $\omega^{i\to i+1}$ the occupancy of sites, which results from ω when a particle at site i hops to site $i+1$:

$$\omega = \{\omega(1), \ldots, \omega(i), \omega(i+1), \ldots, \omega(L)\} \quad \text{and} \tag{1}$$

$$\omega^{i\to i+1} = \{\omega(1), \ldots, \omega(i)-1, \omega(i+1)+1, \ldots, \omega(L)\}. \tag{2}$$

To find stationary distributions of the gradient process, it suffices to enforce the *detailed balance* condition between occupancies

$$\mathbb{P}(\omega)\cdot pf(\omega(i)) = \mathbb{P}(\omega^{i\to i+1})\cdot qf(\omega(i+1)+1), \tag{3}$$

where $\mathbb{P}$ is a probability distribution on occupancies. The left-hand side expresses the rate at which occupancy ω becomes $\omega^{i\to i+1}$, and the right-hand side expresses the rate of the reverse process. Intuitively, if (3) holds for $\mathbb{P}$, the rates at which the gradient process moves between occupancies ω and $\omega^{i\to i+1}$ are perfectly balanced by $\mathbb{P}$. Accordingly, if the gradient particles are distributed according to $\mathbb{P}$, the dynamics are unable to change this; $\mathbb{P}$ is stationary for the gradient process.

2.2.2. Marginal Distributions

Section 2.1 stipulates that gradient particles occupying a common site interact with one another by altering the rate at which they hop to other sites. It therefore seems reasonable to expect that a distribution of particles arising from the dynamics would involve dependencies across some or all sites. However, despite the many interactions between the particles, we can find a probability distribution $\mathbb{P}$ on occupancies ω, which both satisfies (3) and *marginalizes* into independent distributions $\mathbb{P}_i^{\theta_i}$ on single-site occupancies $\omega(i)$. That is, $\mathbb{P}(\omega) = \prod_{i=1}^{L}\mathbb{P}_i^{\theta_i}(\omega(i))$, where θ_i is a parameter of the marginal distribution at site i. This property enables us to study the simpler marginal distributions $\mathbb{P}_i^{\theta_i}$ instead of $\mathbb{P}$ and would not be present if we had instead modeled the hillslope directly, with particles representing units of hillslope height.

The stationary marginal distributions have the form

$$\mathbb{P}_i^{\theta_i}(\omega(i)) = \frac{e^{\theta_i\omega(i)}}{f(\omega(i))!\,Z(\theta_i)} \quad \theta_i\in\mathbb{R}, \tag{4}$$

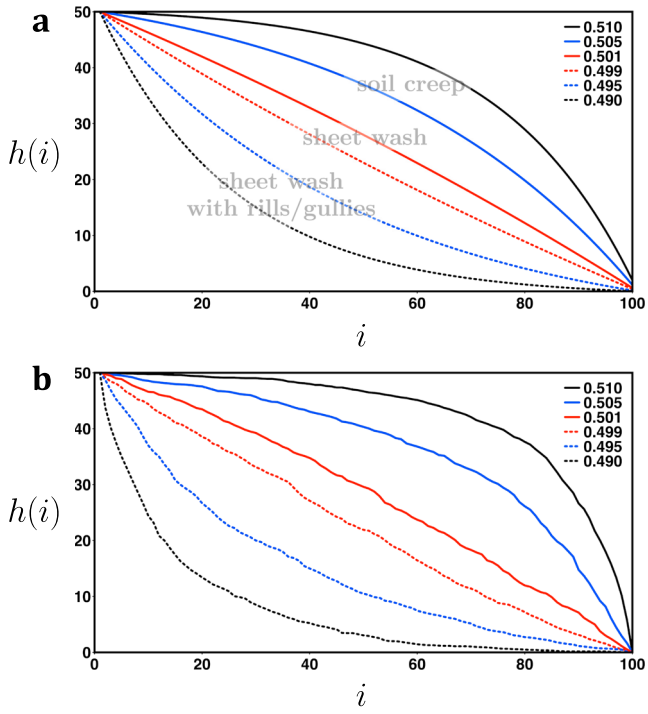

Figure 3. Hillslope profiles produced by the particle model for $f(\omega(i)) = \omega(i)$, fixed $H = 50,\ L = 100$, and values of p shown in the legend, where we fix $p + q = 1$ (a). We indicate soil creep, sheet wash, and sheet wash with rills/gullies as geomorphic processes, which could be modeled by these curves, in analogy with the characteristic-form profiles of Kirkby (1971). Hillslope profiles produced by the particle model for constant rate $f(\omega(i)) = 1$ if $\omega(i) > 0$ (b). We fixed $H = 50,\ L = 100$, and values of p shown in the legend, where we fix $p + q = 1$. The curves represent average profiles obtained over 25 independent, identical simulations of the particle model after $5,000,000$ steps, starting from the stationary profile of the linear rate model with the same choice of p.

with $f(z)! = \prod_{k=1}^{z} f(k)$ and $f(0)! = 1$. $Z(\theta_i) = \sum_{k=0}^{\infty} e^{\theta_i k}/f(k)!$ is a normalization constant, which is assumed to be finite. We note that, if $f(\omega) = 1$ for all ω, then (4) is the familiar geometric distribution; if $f(\omega) = \omega$ for all ω, then (4) is the Poisson distribution. In Appendix A1, we show that (4) indeed satisfies the detailed balance condition of (3), so long as $\exp(\theta_{i+1} - \theta_i) = p/q$. This result motivates the interpretation of the parameter θ_i as relating to the particles' underlying preference for right ($p > 1/2$) or left ($p < 1/2$) jumps.

Using the marginals $\mathbb{P}_i^{\theta_i}$, we would like to calculate the expected number of gradient particles occupying each site in equilibrium. Technically, this quantity depends on the choice of hillslope height H, and so we should calculate the conditional expected number of gradient particles at each site. In equilibrium, for an arbitrary choice of $f(\omega(i))$, parameter θ_i, and fixed height H, the expected number of gradient particles at a site i is

$$\rho^{\theta_i}(i) = \mathbb{E}^{\theta_i}\left(\omega(i) \,\middle|\, \sum_{j=1}^{L} \omega(j) = H\right) = \sum_{k=0}^{H} k \cdot \mathbb{P}^{\theta_i}\left(\omega(i) = k \,|\, \sum_{j=1}^{L} \omega(j) = H\right), \tag{5}$$

where $\mathbb{E}^{\theta_i}$ is the expectation with respect to the distribution $\mathbb{P}^{\theta_i}$ and the notation $\left| \sum \omega = H \right.$ indicates conditioning on the sum of gradient particles being H. The sum over k in (5) is an average over the numbers of gradient particles, which could be at site i, with a weighting based on the probability of observing k particles at site i, subject to the configuration having a total of H gradient particles.

Note that ρ^{θ_i} describes the expected number of particles at each site in equilibrium for the gradient process; it does not describe the number of units of hillslope at each site. In order to obtain the corresponding hillslope profile, we must invert $\omega(i) = h(i) - h(i+1)$ as

$$h(i) = \sum_{j=i}^{L} \omega(j). \tag{6}$$

2.3. Hillslope Profiles for Linear Rate

We can calculate (5) explicitly for the choice of linear rate, $f(\omega(i)) = \omega(i)$, corresponding to the gradient particles hopping with rate proportional to local gradient. For this choice of $f(\omega(i))$ and, as a consequence of (4), the stationary distributions are Poisson

$$\mathbb{P}_i^{\theta_i}(\omega(i)) = \frac{e^{\theta_i \omega(i)} \cdot e^{-e^{\theta_i}}}{\omega(i)!}. \tag{7}$$

In Appendix A2, we show that using (7) with (5) gives

$$\rho^{\theta_i}(i) = H\frac{e^{\theta_i}}{\sum_{j=1}^{L} e^{\theta_j}} = H \cdot \left(\frac{p}{q}\right)^{i-1} \frac{\left(\frac{p}{q}\right) - 1}{\left(\frac{p}{q}\right)^{L} - 1}, \tag{8}$$

where the second equality follows from the stationarity condition $\exp(\theta_{j+1} - \theta_j) = p/q$.

We can invert (8) with $h(i) = \sum_{j=i}^{L} \omega(j)$ to get the corresponding hillslope profile

$$h(i) = H\frac{\left(\frac{p}{q}\right)^{i} - \left(\frac{p}{q}\right)^{L+1}}{\left(\frac{p}{q}\right) - \left(\frac{p}{q}\right)^{L+1}} \quad \text{for} \quad 1 \le i \le L, \tag{9}$$

which describes the expected hillslope profile in equilibrium. Examples of such profiles are provided for a range of p/q values in Figure 3a.

2.4. Hillslope Profiles for Constant Rate

We can also calculate $\rho^{\theta_i}(i) = \mathbb{E}^{\theta_i}\omega(i)$, in absence of conditioning on H, for a choice of constant rate: $f(\omega(i)) = 1$ if $\omega(i) > 0$ and $f(\omega(i)) = 0$ if $\omega(i) = 0$. Whereas, in the case of linear rate, the dynamics depended on the local gradient, the constant rate case corresponds to a dynamics, which evolves steep slopes at the same rate as gradual slopes. The proof of the fact that the conditioning matters little to the stationary hillslope profile is outside the scope of this discussion, and we omit it for brevity.

The occupancies $\omega(i)$ are distributed as geometric random variables, that is,

$$\mathbb{P}_i^{\theta}(\omega(i)) = \frac{e^{\theta_i \omega(i)}}{Z(\theta_i) f(\omega(i))!} = \frac{e^{\theta_i \omega(i)}}{Z(\theta_i)} = e^{\theta_i \omega(i)}(1 - e^{\theta_i}); \tag{10}$$

thus, the expected number of gradient particles has the following simple form

$$\rho^{\theta_i}(i) = \frac{e^{\theta_i}}{1 - e^{\theta_i}}, \tag{11}$$

valid for $(\theta_i < 0)$. The stationary distribution requires $e^{\theta_{i+1} - \theta_i} = p/q$, or

$$e^{\theta_i} = c \cdot \left(\frac{p}{q}\right)^{i} \quad \text{and} \quad i < \frac{-\ln c}{\ln p - \ln q}, \tag{12}$$

where $c > 0$ is a constant determined by (14) and the left boundary condition for height, $h(1) = H$. Combined with (11), we obtain the discrete gradient of the hillslope

$$\rho^{\theta_i}(i) = \frac{c \cdot \left(\frac{p}{q}\right)^{i}}{1 - c \cdot \left(\frac{p}{q}\right)^{i}}. \tag{13}$$

To obtain the expected hillslope profile corresponding to (13), we apply $h(i) = \sum_{j=i}^{L} \omega(j)$ and substitute (13), resulting in

$$h(i) = \sum_{j=i}^{L} \frac{c \cdot \left(\frac{p}{q}\right)^{j}}{1 - c \cdot \left(\frac{p}{q}\right)^{j}}. \tag{14}$$

Hillslope profiles for constant rate and an assortment of choices of p are shown in Figure 3b.

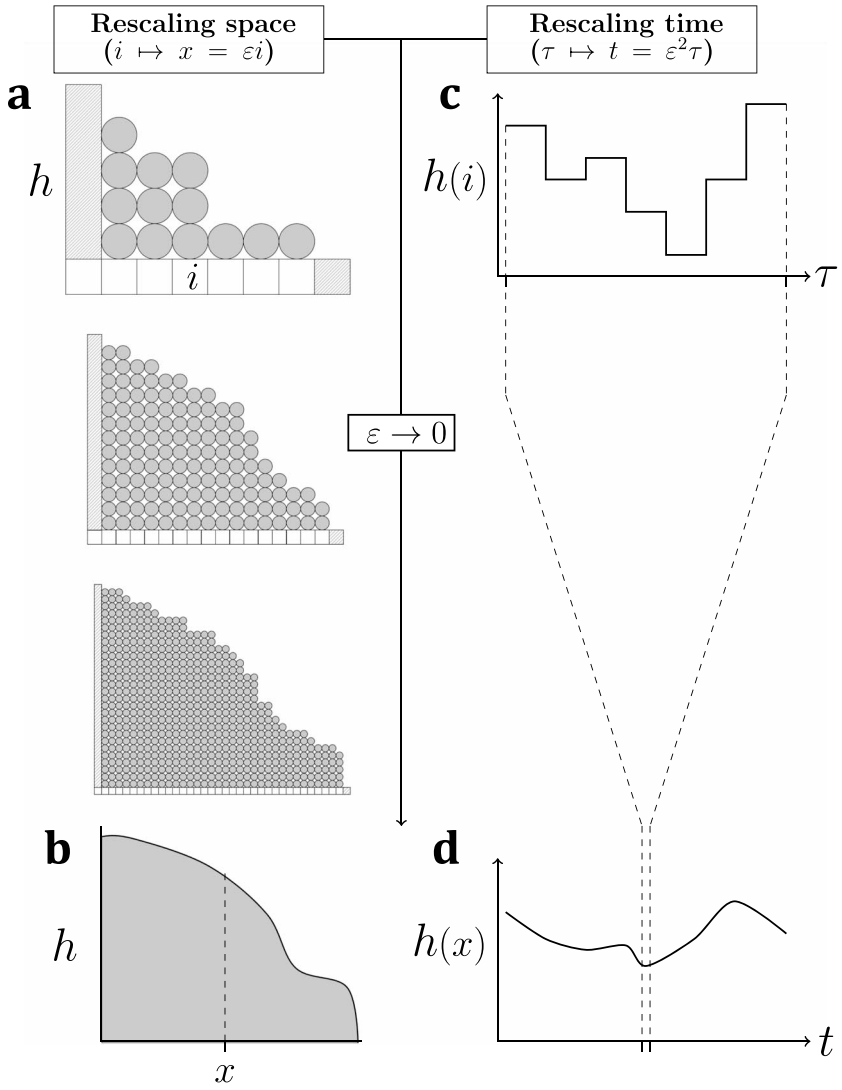

Figure 4. Schematic of space and time rescaling. Discrete space in a particle model of a hillslope, indexed by i (a), is rescaled by a small parameter ε. In the limit as ε approaches 0, discrete space becomes continuous; accordingly, we replace i with a continuous quantity $x = \varepsilon i$ (b). After the rescaling, particles originally spaced by unit distance are spaced by ε. Consider instead the hillslope height at a particular site i, which changes in response to particle movements occurring on a timescale τ (c). After the rescaling of space, changes in hillslope height on timescale τ are too small to be observed, so the dynamics must be quickened by rescaling τ to t with ε^2. Rescaling both space and time results in a macroscopic height $h(x)$ evolving on timescale t (d).

2.5. Particle Model Recap

We recall some key points from section 2 before proceeding to the scaling.

1. The particles of the model represent units of gradient, not units of hillslope.
2. Gradient particles are conserved and have local dynamics; units of hillslope are not conserved (no mass conservation), and the locality/nonlocality of their dynamics is unspecified.
3. Gradient particles move according to a rate function f, which is not necessarily linear.
4. To obtain a hillslope profile, gradient particles must be summed according to (6).
5. Hillslope profiles can be calculated explicitly when f is linear or constant, or simulated otherwise.

3. Heuristic Derivation of the Continuum Equation

We now return to a general setting, where the form of $f(\omega_\tau(i))$ is unspecified, to identify the continuum equation corresponding to the particle-based model of section 2.2. As in section 2.3, the expected number

of gradient particles $\rho_\tau(i) = \mathbb{E}^{\theta_i}\omega_\tau(i)$ is the object of interest, the scaling of which wholly characterizes the gradient process in the limit of macroscopic time and space scales. For simplicity, we consider H fixed, but the scaling argument should hold in cases where H varies slowly in time, relative to the dynamics of the gradient process. We denote the particle model's time by τ and choose the scaling $t = \tau/aL^2$, $x = i/L$, with the interpretation that we *zoom out* by a factor of L and speed up the process by a factor of L^2, in order to observe changes on the new spatial scale. This is the idea expressed in Figure 4, with the small parameter ε chosen in terms of the hillslope length as $\varepsilon = 1/L$, so $\varepsilon \to 0$ as $L \to \infty$. The constant a will become relevant in section 4.3. To suggest their interpretation, we refer to t and τ as times and L as a length; a can be interpreted as a diffusivity. However, we do not consider these quantities to have dimensions, as if we had obtained them through nondimensionalization. In section 4.3, we discuss how these dimensions might be restored. We thus identify the rescaled expected number of gradient particles as

$$\varrho_t(x) := \mathbb{E}^{\rho}\omega_{taL^2}(xL), \tag{15}$$

where the expectation with respect to ρ is justified in Appendix A3.

We require that p and q become increasingly close in value when scaling $\rho_\tau(i)$, in the sense that $p/q \to 1$ as $L \to \infty$. The intuition for this choice comes from the $f(\omega_\tau(i)) = \omega_\tau(i)$ curves of Figure 3a, which indicate that increasing p relative to q results in a profile more closely resembling a step function. The scaling procedure will only serve to accentuate this resemblance and so, to avoid a discontinuous rescaled $\varrho_t(x)$, we choose the *weakly asymmetric* limit, where $p = \frac{1}{2} + \frac{E}{L}$ and $q = \frac{1}{2} - \frac{E}{L}$, and where E is a positive parameter. This scaling is called weakly asymmetric in reference to the symmetric case $p = q$ and to reflect the fact that, for any fixed E, as $L \to \infty$, E/L becomes increasingly small and so p is nearly q. Note that, while our choices force $p > q$, we could just as easily address $p < q$ by swapping them.

We proceed to examine the time evolution of ρ_τ for a site i, with Figure 1b in mind. Particles at site $i-1$ and $i+1$ hop to i with respective rates $pf(\omega_\tau(i-1))$ and $qf(\omega_\tau(i+1))$; particles at site i hop away to sites $i-1$ and $i+1$ with respective rates $qf(\omega_\tau(i))$ and $pf(\omega_\tau(i))$. This is summarized as follows, where the positive terms correspond to those particles hopping to i and the negative terms correspond to those particles hopping from i to adjacent sites

$$\frac{\mathrm{d}}{\mathrm{d}\tau}\rho_\tau(i) = \frac{\mathrm{d}}{\mathrm{d}\tau}\mathbb{E}^{\rho}\omega_\tau(i) \tag{16}$$

$$= \mathbb{E}^{\rho}pf(\omega_\tau(i-1)) + \mathbb{E}^{\rho}qf(\omega_\tau(i+1)) - \mathbb{E}^{\rho}pf(\omega_\tau(i)) - \mathbb{E}^{\rho}qf(\omega_\tau(i)). \tag{17}$$

We now substitute the weak asymmetry condition in the following way

$$\frac{\mathrm{d}}{\mathrm{d}\tau}\mathbb{E}^{\rho}\omega_\tau(i) = -\mathbb{E}^{\rho}f\left(\omega_\tau(i)\right) + \frac{1}{2}\mathbb{E}^{\rho}f\left(\omega_\tau(i+1)\right) \tag{18}$$

$$- \frac{E}{L}\mathbb{E}^{\rho}f\left(\omega_\tau(i+1)\right) + \frac{1}{2}\mathbb{E}^{\rho}f\left(\omega_\tau(i-1)\right) + \frac{E}{L}\mathbb{E}^{\rho}f\left(\omega_\tau(i-1)\right)$$

$$= \frac{1}{2}\left[\mathbb{E}^{\rho}f\left(\omega_\tau(i+1)\right) - 2\mathbb{E}^{\rho}f\left(\omega_\tau(i)\right) + \mathbb{E}^{\rho}f\left(\omega_\tau(i-1)\right)\right] \tag{19}$$

$$- \frac{E}{L}\left[\mathbb{E}^{\rho}f\left(\omega_\tau(i+1)\right) - \mathbb{E}^{\rho}f\left(\omega_\tau(i-1)\right)\right].$$

We continue by defining $G(\rho) := \mathbb{E}^{\rho}f(\omega)$ and substitute the rescaled t and x variables

$$\frac{1}{aL^2}\frac{\partial}{\partial t}\mathbb{E}^{\rho}\omega_{taL^2}(xL) = \frac{1}{2}\left[G\left(\rho_{taL^2}(xL+1)\right) - 2G\left(\rho_{taL^2}(xL)\right) + G\left(\rho_{taL^2}(xL-1)\right)\right] \tag{20}$$

$$- \frac{E}{L}\left[G\left(\rho_{taL^2}(xL+1)\right) - G\left(\rho_{taL^2}(xL-1)\right)\right].$$

Rearranging and identifying $\varrho_t(x)$, we find

$$\frac{\partial}{\partial t}\varrho_t(x) = \frac{aL^2}{2}\left[G\left(\varrho_t\left(x+L^{-1}\right)\right) - 2G\left(\varrho_t(x)\right) + G\left(\varrho_t\left(x-L^{-1}\right)\right)\right] \tag{21}$$

$$- aEL\left[G\left(\varrho_t\left(x+L^{-1}\right)\right) - G\left(\varrho_t\left(x-L^{-1}\right)\right)\right].$$

$$\simeq \frac{a}{2}\frac{\partial^2}{\partial x^2}G(\varrho_t(x)) - 2aE\frac{\partial}{\partial x}G(\varrho_t(x)). \tag{22}$$

We conclude

$$\frac{\partial}{\partial t}\varrho_t(x) \simeq \frac{a}{2}\frac{\partial^2}{\partial x^2}G\left(\varrho_t(x)\right) - 2aE\frac{\partial}{\partial x}G\left(\varrho_t(x)\right). \tag{23}$$

By repeating this argument for the leftmost and rightmost sites (see Appendix A4), we obtain the Robin boundary conditions (a linear combination of Dirichlet and Neumann boundary conditions)

$$\frac{\partial}{\partial x}G\left(\varrho_t(0)\right) = 4EG\left(\varrho_t(0)\right) \quad \text{and} \quad \frac{\partial}{\partial x}G(\varrho_t(1)) = 4EG(\varrho_t(1)). \tag{24}$$

The boundary conditions (24) are consistent with the time-stationary solution of (23), $\varrho(x)$, together implying

$$\frac{\mathrm{d}}{\mathrm{d}x}G(\varrho(x)) = 4EG(\varrho(x)) \quad 0 \le x \le 1, \tag{25}$$

the general solution of which is $G(\varrho(x)) = Ce^{4Ex}$.

Equation (23), along with (24), is the continuum description of the particle-based hillslope model. Appendix A5 describes the solution to (23) subject to the boundary conditions (24). Note that, as in section 2.2, (23) describes the evolution of the gradient process, and so its solutions must be integrated to obtain the corresponding hillslope profiles.

In Appendix A6, we obtain the continuum equation for the evolution of the hillslope profile $h_t(x)$ by substituting $\varrho_t(x) = \frac{\partial}{\partial x}h_t(x)$ into (23) and then integrating. We find that

$$\frac{\partial}{\partial t}h_t(x) = \frac{a}{2}\frac{\partial}{\partial x}G\left(\frac{\partial}{\partial x}h_t(x)\right) - 2aEG\left(\frac{\partial}{\partial x}h_t(x)\right), \tag{26}$$

with boundary conditions given by substituting $\frac{\partial}{\partial x}h_t(x)$ into (24).

3.1. Special Cases of the Continuum Equation

3.1.1. When f is Linear in ω

In the special case of $f(\omega(i)) = \omega(i)$, we have $G(\varrho_t(x)) = \varrho_t(x)$, so the continuum equation is an advection-diffusion equation

$$\frac{\partial}{\partial t}\varrho_t(x) \simeq \frac{a}{2}\frac{\partial^2}{\partial x^2}\varrho_t(x) - 2aE\frac{\partial}{\partial x}\varrho_t(x) \tag{27}$$

with Robin boundary conditions

$$\frac{\partial}{\partial x}\varrho_t(0) = 4E\varrho_t(0) \quad \text{and} \quad \frac{\partial}{\partial x}\varrho_t(1) = 4E\varrho_t(1). \tag{28}$$

Specializing (26), we find that the continuum equation for the hillslope profile h_t is identical to the one for ϱ_t

$$\frac{\partial}{\partial t}h_t(x) \simeq \frac{a}{2}\frac{\partial^2}{\partial x^2}h_t(x) - 2aE\frac{\partial}{\partial x}h_t(x), \tag{29}$$

with boundary conditions by substituting $\frac{\partial}{\partial x}h_t(x)$ into (28).

3.1.2. When f is Constant in ω

In the special case of $f(\omega(i)) = 1$ for $\omega(i) > 0$, $G(\varrho_t(x)) = \varrho_t(x)/(1 + \varrho_t(x))$, so the continuum equation has the following form

$$\frac{\partial}{\partial t}\varrho_t(x) \simeq \frac{a}{2}\frac{\partial^2}{\partial x^2}\frac{\varrho_t(x)}{1+\varrho_t(x)} - 2aE\frac{\partial}{\partial x}\frac{\varrho_t(x)}{1+\varrho_t(x)} \tag{30}$$

with Robin boundary conditions

$$\frac{\partial}{\partial x}\frac{\varrho_t(0)}{1+\varrho_t(0)} = 4E\frac{\varrho_t(0)}{1+\varrho_t(0)} \quad \text{and} \quad \frac{\partial}{\partial x}\frac{\varrho_t(1)}{1+\varrho_t(1)} = 4E\frac{\varrho_t(1)}{1+\varrho_t(1)}. \tag{31}$$

Specializing (26), we find that the corresponding continuum equation for the hillslope profile h_t is

$$\frac{\partial}{\partial t}h_t(x) \simeq \frac{a}{2}\frac{\frac{\partial^2}{\partial x^2}h_t(x)}{\left(1+\frac{\partial}{\partial x}h_t(x)\right)^2} - 2aE\frac{\frac{\partial}{\partial x}h_t(x)}{1+\frac{\partial}{\partial x}h_t(x)}, \tag{32}$$

with boundary conditions given by substituting $\frac{\partial}{\partial x}h_t(x)$ into (31).

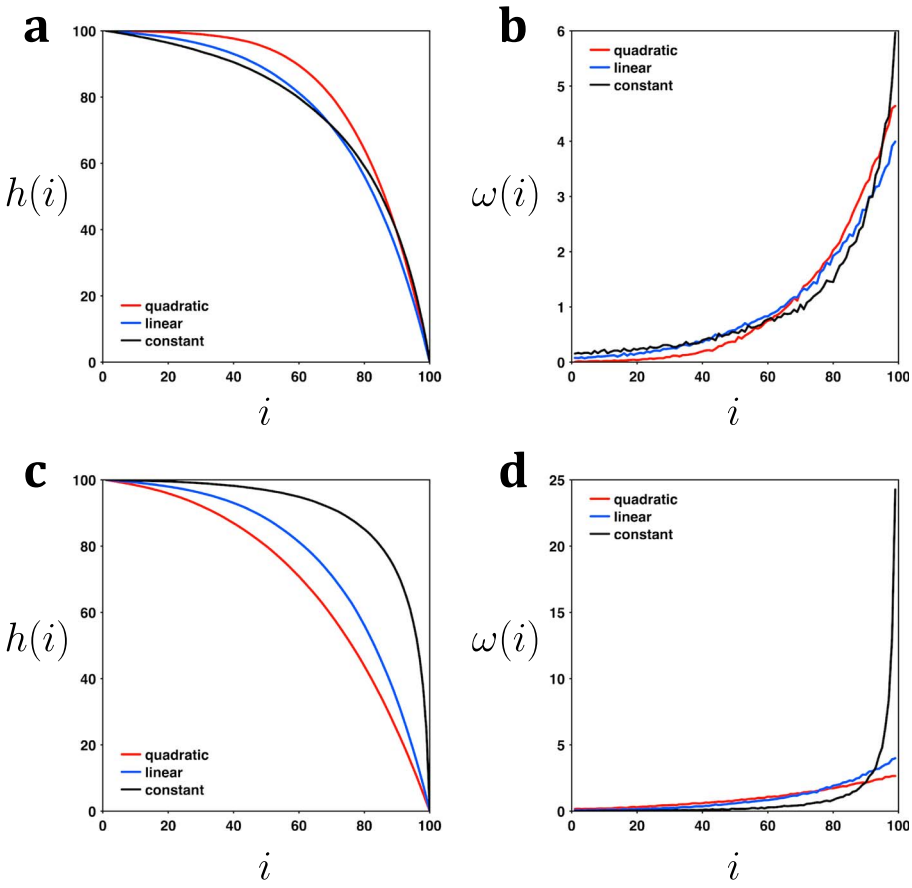

Figure 5. Equilibrium hillslope (a and c) and gradient profiles (b and d) for quadratic $\left(f(\omega)=\omega^2\right)$, linear $\left(f(\omega)=\omega\right)$, and constant $\left(f(\omega)=1 if \omega>0\right)$ rates. For a and b, parameters were $p=0.52$ (quadratic), $p=0.51$ (linear), $p=0.505$ (constant), $H=L=100$. For c and d, parameters were $p=0.51$ (all rates), $H=L=100$. All curves were obtained as the average over 10 identical trials.

3.2. Scaling Recap

We recall some key points from section 3 before describing simulations and dimensionalization.

1. The scaling procedure consists of three steps: balancing incoming and outgoing particles, substituting the weak asymmetry condition, and substituting the rescaled variables.
2. The resulting continuum equation describes the number of gradient particles along the hillslope and is of advection-diffusion type.
3. The continuum equation contains a function G which has simple, explicit forms when the rate function is linear or constant.
4. The scaling argument confirms that, even if the continuum equation is complicated, its solutions can easily be approximated by simulating the corresponding particle model.

4. Simulation and Dimensionalization

The analysis of section 3 tells us that if we want to study the evolution of hillslopes according to (23), we can simulate the particle model of section 2 instead. As choices of rate $f(\omega)\neq\omega$ generally lead to a nonlinear PDE (23), simulating the particle model may often be preferable to an analytic approach or a numerical scheme. In addition to simulating the equilibrium hillslope profiles under various values of p and rate function f, we would also like to simulate the response of hillslopes to perturbations, such as river erosion or climate change (usually implemented by a change in a diffusion coefficient [Fernandes & Dietrich, 1997; Mudd & Furbish, 2004; Roering et al., 2001]). We begin with simulations of equilibrium hillslope profiles.

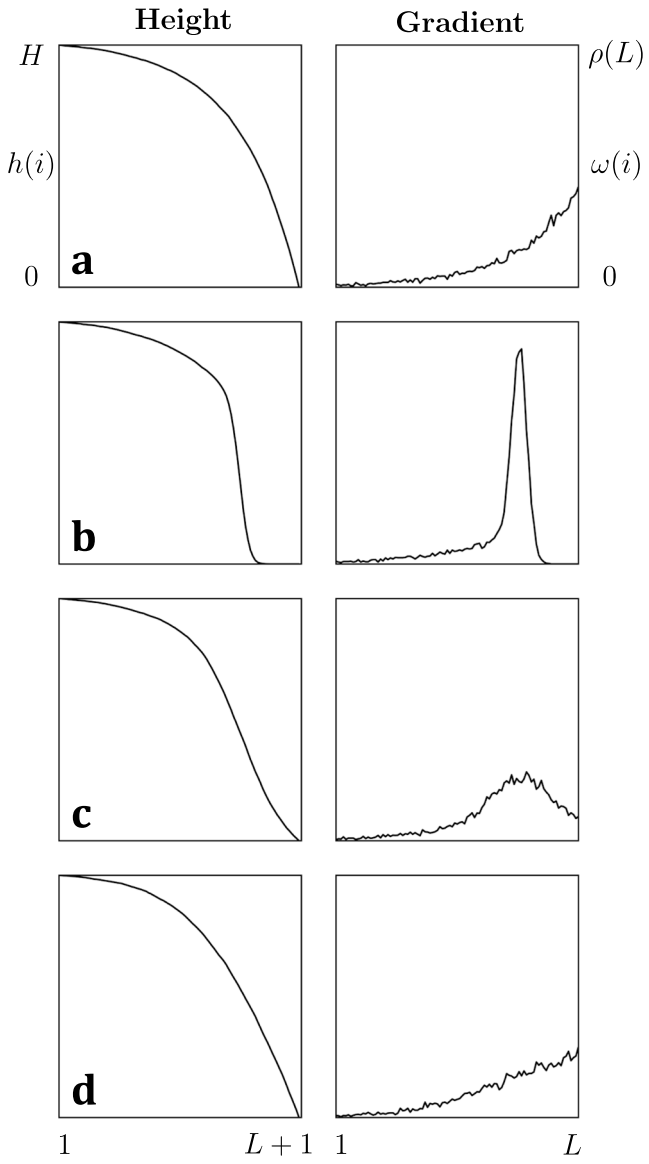

Figure 6. Simulated hillslope response to a river-erosion-like perturbation. A hillslope in equilibrium (a) with linear rate $f(\omega) = \omega$ is perturbed (b) and relaxes (c and d). The rows depict time steps 1×10^6 (a), 1.1×10^6 (b), 2.5×10^6 (c), and 5×10^6 (d), for a perturbation applied near the righthand boundary immediately after time step 1×10^6. The particle model was initialized at equilibrium (equation (9)) with parameters $p = 0.51$, $H = 1 \times 10^4$, and $L = 100$. At equilibrium, $\rho(i)$ is given by (8).

4.1. Equilibrium Hillslope Profiles

When the hopping rates of the gradient process are chosen to be $f(\omega(i)) = \omega(i)$, the hillslope gradients satisfy equation (27). For other choices of rates, the gradients evolve according to equation (23). Balázs and Seppäläinen (2007) showed that convex (concave) $f(\omega(i))$ implies convexity (concavity) of $G(\rho)$. To demonstrate these two cases, we pick constant and quadratic rates given by $\left(f(\omega(i)) = 1 \text{ for } \omega(i) > 0, f(\omega(i)) = 0 \text{ for } \omega(i) = 0\right)$ and $f(\omega(i)) = \omega(i)^2$, respectively. As a result of section 3, the behavior of these solutions can be understood by simulating the corresponding particle model. Stationary hillslope and gradient profiles are compared in Figure 5. In particular, Figures 5a and 5b highlight that, for different choices of p, the profiles arising from linear, quadratic, and constant rates can be made relatively similar, but their curvatures differ. This result echoes comparisons of hillslope forms arising from linear and nonlinear transport (Roering et al., 1999, 2007). Figures 5c and 5d show that, for a given value of p, the profile arising from a constant rate is far steeper than those from linear and quadratic rates. Informally, linear and quadratic rates respond aggressively to large local gradients, leading to a smoother profile than in the case of constant rate. Note that the profiles in the linear rate case can be calculated from (9), while the constant and quadratic results can be produced with the following simulation procedure.

We begin by specifying f, parameters H, L, and p, and the number of simulation time steps, N. We choose an initial height profile, which satisfies the boundary conditions, and use $\omega(i) = h(i) - h(i+1)$ to get the corresponding gradient profile. For each time step, we (i) apply f to each element of ω; (ii) draw random numbers from independent exponential distributions with rates $f(\omega(i))$, respectively representing the time interval until the next hop occurs at site i; (iii) identify the site i with the next hop; and (iv) update ω and h to reflect this hop, contingent on satisfying boundary conditions. We implemented this procedure and conducted all simulations in MATLAB (R2016b, The MathWorks, Inc., Natick, Massachusetts, USA).

4.2. Hillslope Perturbations and Empirical Flux

We now turn our attention to hillslopes perturbed away from equilibrium, to study the timescales over which hillslopes relax and the influence the parameters have over this process. Consider the gradient process with linear rate $f(\omega(i)) = \omega(i)$, $p = 0.51$, $L = 100$, and $H = 1 \times 10^4$. We emphasize that we could choose H so as to make any average slope we wish, but choose a large value of H so the perturbed profiles are smoother. In fact, for the linear rate case, (9) indicates that the shape of the stationary hillslope profile is the same for any H. However, the average slope does affect the relaxation time, with steeper slopes having dynamics at least as fast as those of relatively gradual slopes.

We initialize $\omega(i)$ by calculating $h(i)$ from (9), rounding $h(i)$ to the nearest integer greater than or equal to $h(i)$, and then calculating $\omega(i)$ from the rounded $h(i)$. We introduce a perturbation, which conserves the total number of units of gradient, by skimming 50 such units from each site with at least that many. All of the skimmed particles are then added to a single site. This perturbation is designed to mimic lateral fluvial erosion undercutting the slope base resulting in oversteepening of the hillslope (Harvey, 1994). This scenario can occur during high floods or local response to base-level change upstream. We track $h(i)$ and $\omega(i)$ as the hillslope relaxes back to equilibrium (Figure 6). Figure 6a depicts the hillslope and gradient profiles maintaining equilibrium for 1×10^6 time steps. Figures 6b and 6c show the profiles smoothing and refilling the base at time steps 1.1×10^6 and 2.5×10^6, respectively. By time step 5×10^6, the hillslope resembles the equilibrium hillslope.

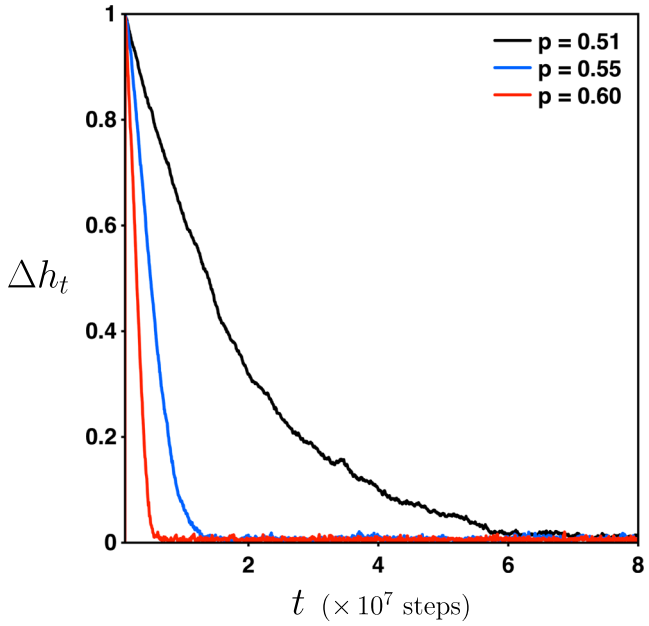

Figure 7. Hillslope profile relaxation in response to a perturbation, for a particle model with $f(\omega(i)) = \omega(i)$, $p = 0.51$, $p = 0.55$, or $p = 0.60$, $H = 1 \times 10^4$, $L = 100$, and $t = 0$ to $t = 8 \times 10^7$. Δh_t (defined by 33) was normalized by its largest value over the simulation. Each curve is the average over 25 trials.

It is natural to wonder about the affect p has on the rate of hillslope relaxation in response to perturbations that do not change the underlying dynamics. Consider the same process, with $p = 0.51$, $p = 0.55$, or $p = 0.60$. Take

$$\Delta h_t(i) := \left|h_t(i) - h_0(i)\right| \qquad \text{and} \qquad \Delta h_t := \sum_{i=1}^{L} \Delta h_t(i) \tag{33}$$

as measures of distance from the h_0 equilibrium. The results for $t = 0$ to $t = 8{\times}10^7$ are shown in Figure 7. It seems that the larger p is, the greater the asymmetry in hopping rates, and the faster the hillslope returns to equilibrium. However, the perturbation depends on the gradient profile, and larger values of p are associated with steeper hillslopes, meaning the local slope is not controlled in the experiment.

To separately test the affects of p and local slope on the rate of hillslope relaxation, we identified contiguous, 10-site regions of equilibrium hillslopes, for various choices of p, which had slope similar to that of an equilibrium profile for a different choice of p (Figures 8a and 8b). We then perturbed these regions of similar slope by adding one quarter of the total number of gradient particles in that region to a single drop site. For the linear rate model, the time series of $\Delta h_t(i)$ (where i was the drop site) were well fit by exponential decays ($R^2 > 0.995$ in all cases) with identical time constants of 1.47×10^{-4} (Figure 8c). We then conducted the same perturbation, but for all possible contiguous 10-site windows. The resulting exponential decays for sites $i = 10, 15, \ldots, 90$ had time constants that agreed with that of Figure 8 and are summarized in (Figure 8d); this result seems to be consistent with the previous findings of exponential decay in topography (Booth et al., 2017). These simulation results suggest that, for linear rate, the timescale over which hillslopes relax does not depend on p or the local slope; this conclusion is in agreement with the calculation of sections A5 and (A33) in particular. We emphasize that this is not the case in general.

We recall that the dynamics of the gradient particle model correspond to deposition and erosion events for the hillslope, but neither the origin of the deposited material nor the destination of the eroded material are specified. In other words, there is no conservation principle for hillslope height. Consequently, fluxes of hillslope height, which would develop during the process of equilibration are not directly accessible via the methods of section 3. However, we can accessorize our particle model with an *empirical* flux inferred from height changes along the hillslope, which depends on observations at times t and $t + \Delta t$. For example, if we assume that growth downslope of a site i requires that a flux arose upslope of site i, we can calculate the empirical flux at site i, relative to time steps t and $t + \Delta t$, as

$$\phi_{t+\Delta t}(i) - \phi_t(i) = r\,\Delta t + \sum_{j>i} \left(h_{t+\Delta t}(j) - h_t(j)\right). \tag{34}$$

Here r is a constant, downhill flux exiting the right boundary and we adopt the convention that a positive value of flux at a site i indicates a net, relative height change for sites $j > i$. Equation (34) describes a nonlocal flux, in the sense that determining the flux through a site i involves consideration of sites other than i. We note that (34) is an integrated Exner equation for our setting.

To demonstrate the use of the empirical flux, we consider a hillslope with $H = 50$ and $L = 100$, initially at equilibrium with $p = 0.55$. For convenience, we choose Δt to be the length of one time step in the simulation. Immediately after $t = 0$, we switch to $p = 0.51$, producing a net flux toward the righthand boundary, as the hillslope equilibrates. To isolate the flux contributions driven by equilibration from those of the constant flux r, we instead track the *cumulative* flux through site i as

$$\bar{\phi}_t(i) := \left|\phi_t(i) - \phi_0(i) - rt\right|. \tag{35}$$

Figure 9a shows the before-and-after hillslope profiles, corresponding to $p = 0.55$ and $p = 0.51$, and Figure 9b shows the cumulative flux through sites $i = 25$, 50, and 75 during equilibration.

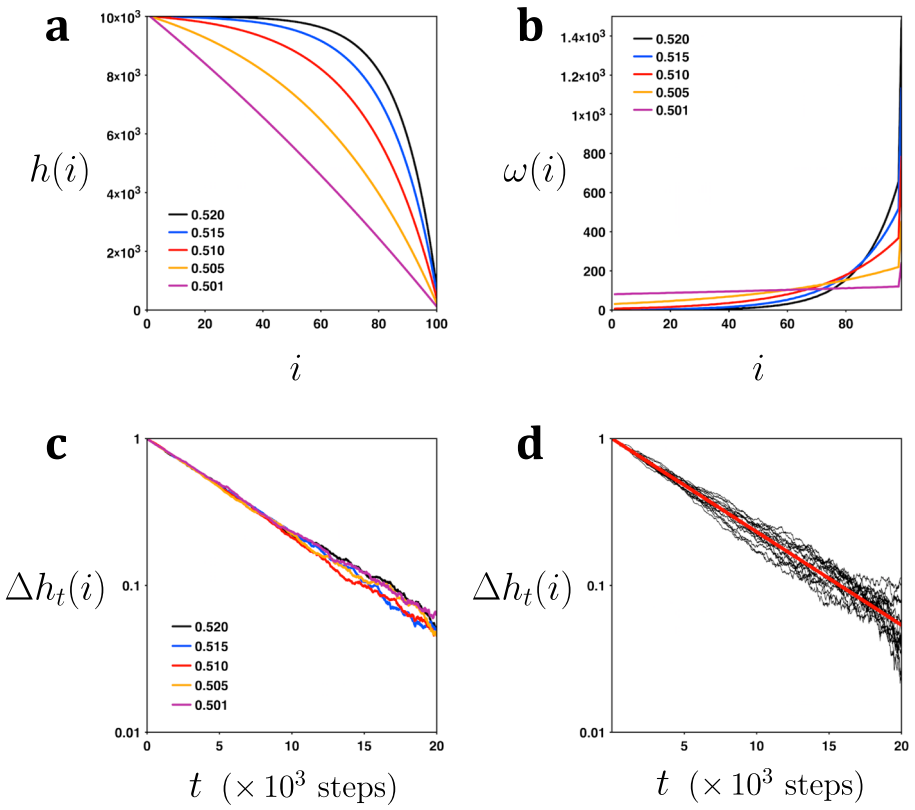

Figure 8. The role of p and gradient on hillslope relaxation in the linear rate model. Equilibrium hillslope profiles for a variety of choices of p (a) and the corresponding gradient profiles (b). Parameters were $H = 1 \times 10^4$ and $L = 100$, with linear rate $f(\omega) = \omega$. The gradient profiles overlap around $i = 70$, so we can control for the affect of local slope on the rate of hillslope relaxation by perturbing in the overlap region. For each choice of p, the perturbation (applied at the beginning of the simulation) consisted of taking one quarter of the gradient particles from each of 10 sites in an interval centered on $i = 70$ and adding them all to the leftmost site in the interval. The resulting time series of $\Delta h_t(i)$ (defined by (33)) were well fit by exponential decay with common time constant 1.47×10^{-4} (c). $R^2 > 0.995$ in all cases. In (d), we fixed $p = 0.51$ and performed the perturbation experiment using a sliding, 10-site window, in order to test various local gradients along the hillslope. The resulting, normalized Δh_t decays for $i = 10, 15, \ldots, 85, 90$ are shown (thin black curves) with the exponential fit superimposed (thick red curve). Each curve in c and d was the average of 25 identical trials. Values for p in a–c are given in the corresponding figure legends.

4.3. Adding Dimensions and Fitting Parameters

In order to reliably translate simulation results into empirically testable predictions, we need a way of assigning dimensions to otherwise dimensionless model quantities (e.g., particle model length L and the length ℓ of an observed hillslope, in meters). Additionally, we need to specify how hillslope data are used to fit model parameters. We suggest the following procedure, which is partly motivated by the calculations in Appendix A5 and partly by (29).

Recall that sites in the particle model of section 2.1 are indexed by $i = 1, 2, \ldots, L$. Let i count the number of sediment grains in the length of the hillslope. We can set L to be the ratio of the hillslope length ℓ to the average diameter of a grain. With h we denote the difference between the hillslope height at the crest and the height at the end of the hillslope (at a length ℓ away from the crest). We can then set H to be the ratio of h to the average diameter of a grain. For example, if the average grain diameter is 2 mm, ℓ is 200 m, and h is 100 m, we set $L = 100,000$ and $H = 50,000$. In this way, we relate dimensionless particle model quantities L and H to observable hillslope quantities with dimension, ℓ and h. As our model does not resolve the distribution of grain sizes, we suggest the use of the diameter of a grain which is considered typical with respect to the distribution of grain sizes. However, grain size should not affect the nature of the limiting behavior, since even larger grains are orders of magnitude smaller than the length-scale of the hillslope. Nevertheless, to explore a distribution of grain sizes, it is possible to conduct multiple experiments using an array of different grain sizes.

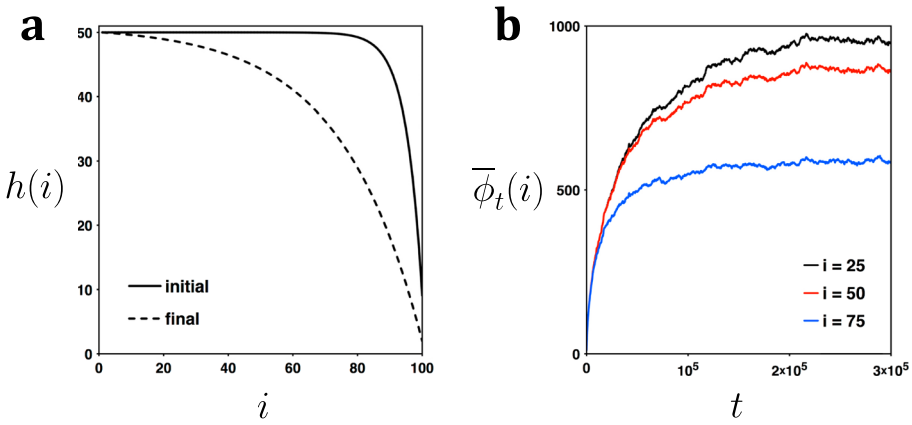

Figure 9. A hillslope equilibrated for $p = 0.55$, $H = 50$, $L = 100$, and linear rate $f(\omega) = \omega$, is perturbed by an abrupt change in the dynamics to $p = 0.51$. In a, the initial profile (solid line) evolves with updated p to the final, equilibrium hillslope (dotted line). In b, cumulative fluxes $\bar{\phi}_t(i)$ (defined by 35) develop in response to the perturbation. Cumulative fluxes averaged over 50 identical trials are shown for sites $i = 25$, $i = 50$, and $i = 75$.

We now consider fitting E, which encapsulates the asymmetry in the underlying gradient process. Ideally, we would observe an individual hillslope in equilibrium and fit E according to the linear rate case (A25). As such an observation is presumably rare and the simulation cost is low, we instead suggest fitting E to different hillslopes and then performing simulations for a range of values of E. This can similarly be done for nonlinear rate models using the contents of Appendix A5.2. The process of finding an appropriate rate function may require trial and error, potentially starting from the constant, linear, and quadratic rate functions of Figure 5.

The process of adding dimension to the time steps is more challenging. Ideally, having determined E and in the context of (29), we would add a small perturbation to the hillslope, the relaxation of which obeys (A33) and from which a could be inferred. However, without experimental innovation or a theoretical work-around, this is impractical. As the development of such an experimental methodology is outside the scope of the present study, we provide this suggestion as a placeholder.

To summarize, we suggest the following, three-step approach:

1. Measure typical grain diameter to add units to H and L.
2. Fit range of E values to observed hillslope shapes.
3. Fit a to hillslope relaxation in response to a perturbation.

While the first step does not depend on the choice of rate function, the second and third steps do, as the form of the rate affects the relationship between E and hillslope shape, and may affect the relationship between a and the coefficients of the advection-diffusion equation for the hillslope height. We also note that this procedure makes use of both small-scale and large-scale measurements, as well as information about hillslope equilibrium and nonequilibrium.

4.4. Simulation Recap

We collect some key points from section 4 before continuing on to the discussion.

1. We simulated perturbations in two ways: rearranging the gradient particles (through ω) and changing the dynamics (through p or, equivalently, E).
2. Hillslope relaxation in response to perturbation can be tracked by comparing it with the corresponding stationary profile or by tracking the empirical fluxes.
3. In the linear rate case, hillslope relaxation timescale is independent of E, H, and L.
4. We suggested the procedure of section 4.3 to assign dimensions to simulation results, but the fitting of diffusivity a may require experimental innovation or a theoretical work-around.

5. Discussion and Conclusion

We have presented a mathematical argument for deriving a continuum description of hillslope erosion, which remains faithful to the particle-scale dynamics that operate over short temporal and spatial scales. The key ingredient of the particle model of section 2 is indirection: the decision for particles to represent units of

hillslope gradient, instead of units of hillslope height. Consider again the scenario of Figure 1. Had we specified similar dynamics on the hillslope profile directly, the resulting profiles could be unrealistic (e.g., large particle buildup next to sites with no particles) and the dynamics would require awkward constraints to prevent such profiles. Most importantly, this process would not have stationary profiles that are amenable to analysis, and a scaling argument like that of section 3 would not apply. In this sense, the gradient particle model is a natural choice, but one made at the expense of direct access to information about sediment flux and particle hopping distances. Indeed, although we can obtain the hillslope profile from the gradient particle profile (using (6)), our model does not prescribe a dynamics on the hillslope profile and so is agnostic to fluxes of units of hillslope and the distances they typically travel. Critically, this circumvents the issue of specifying whether transport on the hillslope is local or nonlocal and, as a result, our model can represent a variety of geomorphic processes and the scaling argument holds across transport regimes.

We are free to accessorize our model with fluxes, defined in terms of hillslope gradient, which evolve according to the particle model of section 2 or, in the continuum, according to (23). In section 4.2, for example, we proposed a nonlocal flux (34) in terms of changes in the hillslope height (equivalently, changes in hillslope gradient via (6)). Alternatively, we could specify a local flux like those of Culling (1963; linear dependence on slope), Andrews and Bucknam (1987; nonlinear dependence on slope), and Furbish, Childs, et al. (2009; nonlinear, includes height and slope), or a nonlocal flux of the form favored by Furbish, Haff, et al. (2013). This freedom reflects the *hillslope-first* nature of our particle model, for which we formulate the dynamics of the hilllslope gradients and infer the flux, as opposed to formulating the dynamics of the flux, from which we then infer the hillslope profile. It is for this reason we have not recovered from our model a GTL, which connects flux to powers of slope (Carson & Kirkby, 1972; Ganti et al., 2012). The analogous law for our model is $G(\rho)$ which, being the expectation of a function f of gradient ω, resembles a traditional GTL and similarly aims to capture the underlying process mechanics.

A hillslope-first approach may be more natural than a nonlocal, transport-first approach for conducting perturbation simulations like those described in section 4.2. For example, consider the experiment illustrated by Figures 6 and 7, which simulates hillslope recovery from river erosion. Nonlocal formulations of transport require as input a distribution of particle travel distances, which must specify the dependence of travel distance on gradient (Furbish & Haff, 2010), or an assumption about the degree of nonlocality (Foufoula-Georgiou et al., 2010), which similarly depends on gradient and so must vary throughout the experiment (Gabet & Mendoza, 2012). In contrast, our model fixes the law governing the redistribution of hillslope gradient through the rate function f, which is an input of the modeler. However, as described in section 4.3, to translate simulation time steps into the timescale of a hillslope under study requires the fitting of diffusivity a which, barring a theoretical work-around, may require experimental innovation.

Given a choice of f, the parameter p can be determined from an observation of hillslope shape, according to the procedure described in section 4.3. Intuitively, for a given rate function and relative to a linear hillslope of the same height and length, $p > \frac{1}{2}$ specifies steeper slopes farther from the crest; $p < \frac{1}{2}$ specifies steeper slopes nearer the crest. For example, in Figure 3a, $p = 0.49$ produces a stationary hillslope profile resembling one formed under sheet wash with gullies, while $p = 0.51$ results in a profile that more closely resembles one formed under soil creep. The parameter p can also be used to conduct perturbation experiments, as in Figure 9, where the hillslope begins as the stationary profile under a process associated with $p = 0.51$ and must equilibrate after an external driver (e.g., climate change) alters the dynamics to $p = 0.55$. It is possible to use a nonlocal, transport-first approach to conduct similar experiments, for example, by making a small change to the volumetric entrainment rate or distribution of particle travel distances.

The particle-based model of section 2 is purely probabilistic, unlike those of Kirkby and Statham (1975) and Gabet and Mendoza (2012), which incorporate frictional forces associated with particle motion, and that of DiBiase et al. (2017), which also accounts for variations in grain size and is extended to motion in two spatial dimensions. These approaches benefit from directly incorporating hillslope microtopography but are computationally expensive in a way which may prohibit the simulation of hillslope evolution over long timescales (DiBiase et al., 2017) and cannot be scaled to corresponding continuum equations (Ancey et al., 2015). Our model is most similar to that of Tucker and Bradley (2010), which is also purely probabilistic, rules-based, and computationally inexpensive, but for which a corresponding continuum description is unavailable.

The scaling argument of section 3 claims that, under the appropriate scalings of time and space variables, and in the limit as $L \to \infty$, the model behaves according to an advection-diffusion equation. Note that

this governs the scaled gradient process, not the hillslope itself—we must integrate the solutions to obtain the corresponding hillslope. For the linear rate case, we can solve the continuum equation directly; in the nonlinear rate case, numerical methods may be required. Both the scaling argument and the resulting continuum equation are general; they hold for any nonnegative, nondecreasing rate function f. Of course, if f is complicated, so too will the continuum equation be (as in Appendix A5.2), and simulating the corresponding particle model will likely be preferable. We emphasize that the scaling procedure both identifies a continuum model, as well as justifies the continuum model's approximation by simulations of the particle model, assuming L is relatively large. The dimensionalization procedure of section 4.3 confirms that this condition will be satisfied in practice, as typical values for grain diameter and hillslope length give $L = 10^5$.

We anticipate that the modeling approach described here will be particularly useful for long-timescale simulations and simulations of landscape relaxation in response to perturbations. As simulations of the particle model are easy to implement and computationally inexpensive, they could be used to evaluate the long-term impact of external drivers or could be incorporated as one component of a larger 1-D model (e.g., hillslope with runoff into a river) while respecting modest computational resources. In addition, the simplicity of the particle model makes it possible to simulate the interaction of sophisticated perturbations, such as intermittent weather patterns or avalanching, with baseline geomorphic processes. Equipped with the dimensionalization procedure, these simulations can be informed by observations of individual grains and entire hillslopes, as well as stationary and perturbed hillslopes, and ultimately translated into concrete predictions.

Appendix A: Mathematical Details

A1. The Product of One-Parameter Marginal Distributions Satisfies Detailed Balance

Following the argument of Balázs and Bowen (2016), we show that the product distribution of (4) satisfies the detailed balance condition given in (3), for bulk sites $i \neq 1, L$; the boundary cases follow from a similar argument.

$$p f(\omega(i))\, \mathbb{P}_i^{\theta_i}(\omega(i))\, \mathbb{P}_{i+1}^{\theta_{i+1}}(\omega(i+1)) \prod_{j \neq i, i+1} \mathbb{P}_j^{\theta_j} \tag{A1}$$

$$= q f(\omega(i+1)+1)\, \mathbb{P}_i^{\theta_i}(\omega(i)-1)\, \mathbb{P}_{i+1}^{\theta_{i+1}}(\omega(i+1)+1) \prod_{j \neq i, i+1} \mathbb{P}_j^{\theta_j}$$

$$p f(\omega(i)) \frac{e^{\theta_i \omega(i)}}{f(\omega(i))!\, Z(\theta_i)} \frac{e^{\theta_{i+1}\omega(i+1)}}{f(\omega(i+1))!\, Z(\theta_{i+1})} \tag{A2}$$

$$= q f(\omega(i+1)+1) \frac{e^{\theta_i(\omega(i)-1)}}{f(\omega(i)-1)!\, Z(\theta_i)} \frac{e^{\theta_{i+1}(\omega(i+1)+1)}}{f(\omega(i+1)+1)!\, Z(\theta_{i+1})}$$

$$p f(\omega(i)) = q f(\omega(i+1)+1) \frac{e^{\theta_{i+1}}}{f(\omega(i+1)+1)} \frac{f(\omega(i))}{e^{\theta_i}} \tag{A3}$$

$$p f(\omega(i)) = q f(\omega(i)) e^{(\theta_{i+1}-\theta_i)}. \tag{A4}$$

The last equation is satisfied when $\exp(\theta_{i+1} - \theta_i) = p/q$ and shows that the product distribution satisfies the bulk reversibility equations.

A2. The Expected Occupancy for $f(\omega(i)) = \omega(i)$

If X_i are independent Poisson random variables with respective parameters λ_i then, for $Y = \sum_{i=1}^n X_i$, the following argument shows $X_i | Y = k$ is binomially distributed with parameters k and $\lambda_i / \sum_{j=1}^n \lambda_j$. Y is the sum of independent Poisson random variables, so it is also Poisson and has parameter $\mu = \sum_{i=1}^m \lambda_i$. Call $Z_i = \sum_{j \neq i} X_j$, which is Poisson with parameter $\mu - \lambda_i$.

$$\mathbb{P}(X_i = m | Y = k) = \frac{\mathbb{P}(X_i = m \cap Y = k)}{\mathbb{P}(Y = k)} \tag{A5}$$

$$= \frac{\mathbb{P}(X_i = m) \cdot \mathbb{P}(Z_i = k - m)}{\mathbb{P}(Y = k)} \tag{A6}$$

$$= \frac{\lambda_i^m e^{-\lambda_i}}{m!} \frac{(\mu - \lambda_i)^{k-m} e^{-(\mu - \lambda_i)}}{(k-m)!} \frac{k!}{\mu^k e^{-\mu}} \tag{A7}$$

$$= \binom{k}{m}\left(\frac{\lambda_i}{\mu}\right)^m\left(\frac{\mu-\lambda_i}{\mu}\right)^{k-m}, \tag{A8}$$

where we used the independence of X_i and Z_i to get from the first line to the second.

Because the stationary distributions $\mathbb{P}_i^{\theta_i}$ are Poisson when $f(\omega(i)) = \omega(i)$, we can apply this fact to (8) as

$$\rho(i)^{\theta_i} = \mathbb{E}^{\theta_i}\left(\omega(i)\,\middle|\,\sum_{j=1}^{L}\omega(j) = H\right) = \sum_{\omega(i)=0}^{H}\omega(i)\cdot\mathbb{P}_i^{\theta_i}\left(\omega(i)\,\middle|\,\sum_{j=1}^{L}\omega(j) = H\right). \tag{A9}$$

We identify (A9) as the mean of a binomial distribution with parameters H and $e^{\theta_i}/\sum_{j=1}^{L}e_j^{\theta}$ to conclude

$$\rho(i)^{\theta_i} = H\frac{e^{\theta_i}}{\sum_{j=1}^{L}e^{\theta_j}}. \tag{A10}$$

A3. $\rho(i)$ is a Strictly Increasing Function of θ_i

As $\rho(i)$ is an observable quantity, but θ_i is not, it is preferable that we parametrize expectations with $\rho(i)$ in the continuum limit. To do so, we need to show that their relation is invertible. It suffices for us to show that $\rho(i)$ is a strictly increasing function of θ_i.

$$\rho(i)^{\theta_i} = \mathbb{E}^{\theta_i}(\omega(i)) = \sum_{k=0}^{\infty}\frac{k\cdot e^{\theta_i k}}{f(k)!\,Z(\theta_i)} \tag{A11}$$

and so

$$\frac{\mathrm{d}}{\mathrm{d}\theta}\rho(i)^{\theta_i} = \sum_{k=0}^{\infty}\frac{k^2\cdot e^{\theta_i k}}{f(k)!\,Z(\theta_i)} - \sum_{k=0}^{\infty}\frac{k\cdot e^{\theta_i k}}{f(k)!\,Z(\theta_i)}\cdot\frac{\frac{\mathrm{d}}{\mathrm{d}\theta_i}Z(\theta_i)}{Z(\theta_i)} \tag{A12}$$

$$= \sum_{k=0}^{\infty}\frac{k^2\cdot e^{\theta_i k}}{f(k)!\,Z(\theta_i)} - \left(\sum_{k=0}^{\infty}\frac{k\cdot e^{\theta_i k}}{f(k)!\,Z(\theta_i)}\right)^2 \tag{A13}$$

$$= \mathbb{E}^{\theta_i}\left(\omega(i)^2\right) - \left(\mathbb{E}^{\theta_i}(\omega(i))\right)^2 > 0 \quad \forall\,\omega(i). \tag{A14}$$

As $\rho(i)^{\theta_i}$ is a strictly increasing function of θ_i, we can invert it to get $\theta_i(\rho(i))$ and so can parametrize expectations in terms of an observable ρ.

A4. Heuristic Scaling of the Boundary Conditions

To find the proper boundary conditions for (23), we repeat the scaling argument for the leftmost site

$$\frac{\partial}{\partial\tau}\mathbb{E}^{\rho}\omega_\tau(1) = \frac{1}{2}\left[\mathbb{E}^{\rho}f(\omega_\tau(2)) - \mathbb{E}^{\rho}f(\omega_\tau(1))\right] - \frac{E}{L}\left[\mathbb{E}^{\rho}f(\omega_\tau(2)) + \mathbb{E}^{\rho}f(\omega_\tau(1))\right], \tag{A15}$$

which implies

$$\frac{1}{L}\frac{\partial}{\partial t}\varrho_t(L^{-1}) = \frac{aL}{2}\left[G\left(\varrho_t\left(2L^{-1}\right)\right) - G\left(\varrho_t\left(L^{-1}\right)\right)\right] - aE\left[G\left(\varrho_t\left(2L^{-1}\right)\right) + G\left(\varrho_t\left(L^{-1}\right)\right)\right] \tag{A16}$$

$$\simeq \frac{a}{2}\frac{\partial}{\partial x}G\left(\varrho_t(0)\right) - 2aEG\left(\varrho_t(0)\right). \tag{A17}$$

In the limit as $L\to\infty$, the $\frac{\partial}{\partial t}$ term drops out and we have the Robin boundary condition

$$\frac{\partial}{\partial x}G\left(\varrho_t(0)\right) = 4EG\left(\varrho_t(0)\right). \tag{A18}$$

Similarly, we obtain the following boundary condition for the rightmost site

$$\frac{\partial}{\partial\tau}\mathbb{E}^{\rho}\omega_\tau(L) = \frac{1}{2}\left[\mathbb{E}^{\rho}f(\omega_\tau(L-1)) - \mathbb{E}^{\rho}f(\omega_\tau(L))\right] + \frac{E}{L}\left[\mathbb{E}^{\rho}f(\omega_\tau(L-1)) + \mathbb{E}^{\rho}f(\omega_\tau(L))\right], \tag{A19}$$

which implies

$$\frac{1}{L}\frac{\partial}{\partial t}\varrho_t(1) = \frac{aL}{2}\left[G\left(\varrho_t\left(1-L^{-1}\right)\right) - G\left(\varrho_t(1)\right)\right] + aE\left[G\left(\varrho_t\left(1-L^{-1}\right)\right) + G\left(\varrho_t(1)\right)\right] \tag{A20}$$

$$\simeq -\frac{a}{2}\frac{\partial}{\partial x}G(\varrho_t(1)) + 2aEG(\varrho_t(1)). \tag{A21}$$

In the limit $L\to\infty$,

$$\frac{\partial}{\partial x}G(\varrho_t(1)) = 4EG(\varrho_t(1)). \tag{A22}$$

A5. Solving the Continuum Equation

We consider the setting of section 3 and, in particular, the continuum equation with Robin boundary conditions

$$\begin{aligned}\frac{\partial}{\partial t}\varrho_t(x) &= \frac{a}{2}\frac{\partial^2}{\partial x^2}G\left(\varrho_t(x)\right) - 2aE\frac{\partial}{\partial x}G\left(\varrho_t(x)\right),\\ \frac{\partial}{\partial x}G\left(\varrho_t(0)\right) &= 4EG\left(\varrho_t(0)\right),\\ \frac{\partial}{\partial x}G\left(\varrho_t(\ell)\right) &= 4EG\left(\varrho_t(\ell)\right).\end{aligned} \tag{A23}$$

A5.1. The Linear Case

When the rates f are linear, G becomes the identity function and the above turns into the constant coefficient advection-diffusion equation

$$\begin{aligned}\frac{\partial}{\partial t}\varrho_t(x) &= \frac{a}{2}\frac{\partial^2}{\partial x^2}\varrho_t(x) - 2aE\frac{\partial}{\partial x}\varrho_t(x),\\ \frac{\partial}{\partial x}\varrho_t(0) &= 4E\varrho_t(0),\\ \frac{\partial}{\partial x}\varrho_t(\ell) &= 4E\varrho_t(\ell).\end{aligned} \tag{A24}$$

Notice that the time-stationary solution of (A24) that we need is $\varrho(x) = \frac{4Eh}{1-e^{4E\ell}}e^{4Ex}$. This is because the rescaled height profile then becomes

$$h(x) = \lim_{L\to\infty}\frac{1}{L}\sum_{i=\lfloor xL\rfloor}^{L}\rho(i) = \lim_{L\to\infty}\sum_{i=\lfloor xL\rfloor}^{L}\varrho\left(\frac{i}{L}\right)\frac{1}{L} = \int_x^\ell \varrho(z)\,\mathrm{d}z = \frac{h}{1-e^{4E\ell}}\left(e^{4Ex}-e^{4E\ell}\right) \tag{A25}$$

as needed for boundary conditions 0 at $x = \ell$ and rescaled height h at $x = 0$. We now introduce the perturbation

$$\bar{\varrho}_t(x) = \varrho_t(x) - \varrho(x) \tag{A26}$$

and notice that this also satisfies (A24). However, it now makes physical sense to start with small initial data $\bar{\varrho}_0(x)$.

As (A24) describes a diffusion with a drift, it is natural to introduce

$$u_t(y) = \bar{\varrho}_t(y + 2aEt), \qquad -2aEt \le y \le 1 - 2aEt. \tag{A27}$$

Then

$$\bar{\varrho}_t(x) = u_t(x - 2aEt), \qquad \frac{\partial}{\partial t}\bar{\varrho}_t(x) = \frac{\partial}{\partial t}u_t(x - 2aEt) - 2aE\frac{\partial}{\partial x}u_t(x - 2aEt), \tag{A28}$$

$$\frac{\partial}{\partial x}\bar{\varrho}_t(x) = \frac{\partial}{\partial x}u_t(x - 2aEt), \qquad \frac{\partial^2}{\partial x^2}\bar{\varrho}_t(x) = \frac{\partial^2}{\partial x^2}u_t(x - 2aEt), \tag{A29}$$

and (A24) becomes

$$\frac{\partial}{\partial t}u_t(y) = \frac{a}{2}\frac{\partial^2}{\partial y^2}u_t(y), \tag{A30}$$

$$\frac{\partial}{\partial y}u_t(-2aEt) = 4Eu_t(-2aEt), \tag{A31}$$

$$\frac{\partial}{\partial y}u_t(1 - 2aEt) = 4Eu_t(1 - 2aEt). \tag{A32}$$

The first line is the ordinary heat equation, while the boundary conditions become rather unusual. As these are satisfied by $u_t(y) \equiv 0$, we expect that at least for times much smaller than $\frac{1}{2aE}$ the boundary will not play a significant role in the solution if the initial condition u_0 is small. Hence, the solution should be close to

$$\begin{aligned}u_t(y) &= \frac{1}{\sqrt{2\pi at}}\int_{-\infty}^{\infty} e^{-\frac{(y-z)^2}{2at}}u_0(z)\,\mathrm{d}z, \qquad \text{or}\\ \bar{\varrho}_t(x) = u_t(x - 2aEt) &= \frac{1}{\sqrt{2\pi at}}\int_{-\infty}^{\infty} e^{-\frac{(x-2aEt-z)^2}{2at}}\bar{\varrho}_0(z)\,\mathrm{d}z.\end{aligned} \tag{A33}$$

A5.2. The Nonlinear Case

Here we consider a general but smooth G with derivative $G' > 0$ bounded away from 0 in the relevant range of densities. G and G' are often not explicit but enjoy pleasant properties for particular models. The time-stationary solution of (A23) is $G(\varrho(x)) = ce^{4Ex}$ with a constant c that gives

$$h = \int_0^1 \varrho(z)\,\mathrm{d}z = \int_0^1 G^{-1}\left(ce^{4Ez}\right)\,\mathrm{d}z = \frac{1}{4E}\int_{G^{-1}(c)}^{G^{-1}(ce^{4E})} v\,(\ln G(v))'\,\mathrm{d}v. \tag{A34}$$

Notice that this solves

$$\frac{1}{2}\frac{\partial^2}{\partial x^2}G(\varrho(x)) = 2E\frac{\partial}{\partial x}G(\varrho(x)), \tag{A35}$$

$$\frac{\partial}{\partial x}G(\varrho(0)) = 4EG(\varrho(0)), \tag{A36}$$

$$\frac{\partial}{\partial x}G(\varrho(\ell)) = 4EG(\varrho(\ell)), \tag{A37}$$

that is,

$$\begin{aligned}\frac{1}{2}G''(\varrho(x))\left(\frac{\partial}{\partial x}\varrho(x)\right)^2 + \frac{1}{2}G'(\varrho(x))\frac{\partial^2}{\partial x^2}\varrho(x) &= 2EG'(\varrho(x))\frac{\partial}{\partial x}\varrho(x),\\ G'(\varrho(0))\frac{\partial}{\partial x}\varrho(0) &= 4EG(\varrho(0)),\\ G'(\varrho(\ell))\frac{\partial}{\partial x}\varrho(\ell) &= 4EG(\varrho(\ell)).\end{aligned} \tag{A38}$$

As above, let

$$\bar{\varrho}_t(x) = \varrho_t(x) - \varrho(x) = \varrho_t(x) - G^{-1}\left(ce^{4Ex}\right). \tag{A39}$$

Assuming this (and its derivatives) are small, we have

$$\frac{\partial}{\partial t}\varrho_t(x) = \frac{\partial}{\partial t}\bar{\varrho}_t(x), \tag{A40}$$

$$G\left(\varrho_t(x)\right) = G(\varrho(x)) + G'(\varrho(x))\cdot\bar{\varrho}_t(x) + \mathcal{O}\left(\bar{\varrho}_t(x)\right)^2, \tag{A41}$$

$$\frac{\partial}{\partial x}G\left(\varrho_t(x)\right) = G'\left(\varrho_t(x)\right)\frac{\partial}{\partial x}\varrho_t(x) \tag{A42}$$

$$= G'(\varrho(x))\left(\frac{\partial}{\partial x}\bar{\varrho}_t(x) + \frac{\partial}{\partial x}\varrho(x)\right) \tag{A43}$$

$$+ G''(\varrho(x))\cdot\bar{\varrho}_t(x)\cdot\left(\frac{\partial}{\partial x}\bar{\varrho}_t(x) + \frac{\partial}{\partial x}\varrho(x)\right) + \mathcal{O}\left(\bar{\varrho}_t(x)\right)^2$$

$$= G'(\varrho(x))\left(\frac{\partial}{\partial x}\bar{\varrho}_t(x) + \frac{\partial}{\partial x}\varrho(x)\right) \tag{A44}$$

$$+ G''(\varrho(x))\cdot\bar{\varrho}_t(x)\cdot\frac{\partial}{\partial x}\varrho(x) + \mathcal{O}\left(\bar{\varrho}_t(x)\right)^2,$$

$$\frac{\partial^2}{\partial x^2}G\left(\varrho_t(x)\right) = G''\left(\varrho_t(x)\right)\left(\frac{\partial}{\partial x}\varrho_t(x)\right)^2 + G'\left(\varrho_t(x)\right)\frac{\partial^2}{\partial x^2}\varrho_t(x) \tag{A45}$$

$$= G''(\varrho(x))\left(\frac{\partial}{\partial x}\bar{\varrho}_t(x) + \frac{\partial}{\partial x}\varrho(x)\right)^2 \tag{A46}$$

$$\begin{aligned}&+ G'''(\varrho(x))\cdot\bar{\varrho}_t(x)\cdot\left(\frac{\partial}{\partial x}\bar{\varrho}_t(x) + \frac{\partial}{\partial x}\varrho(x)\right)^2\\ &+ G'(\varrho(x))\left(\frac{\partial^2}{\partial x^2}\bar{\varrho}_t(x) + \frac{\partial^2}{\partial x^2}\varrho(x)\right)\\ &+ G''(\varrho(x))\cdot\bar{\varrho}_t(x)\cdot\left(\frac{\partial^2}{\partial x^2}\bar{\varrho}_t(x) + \frac{\partial^2}{\partial x^2}\varrho(x)\right) + \mathcal{O}\left(\bar{\varrho}_t(x)\right)^2\\ &= G''(\varrho(x))\left(\frac{\partial}{\partial x}\bar{\varrho}_t(x) + \frac{\partial}{\partial x}\varrho(x)\right)^2 + G'''(\varrho(x))\cdot\bar{\varrho}_t(x)\cdot\left(\frac{\partial}{\partial x}\varrho(x)\right)^2\\ &+ G'(\varrho(x))\left(\frac{\partial^2}{\partial x^2}\bar{\varrho}_t(x) + \frac{\partial^2}{\partial x^2}\varrho(x)\right) + G''(\varrho(x))\cdot\bar{\varrho}_t(x)\cdot\frac{\partial^2}{\partial x^2}\varrho(x) + \mathcal{O}\left(\bar{\varrho}_t(x)\right)^2.\end{aligned} \tag{A47}$$

Combine this with (A23) and (A38) to obtain

$$\frac{\partial}{\partial t}\bar{\varrho}_t(x) = \frac{a}{2}G'\left(\varrho(x)\right)\cdot\frac{\partial^2}{\partial x^2}\bar{\varrho}_t(x) \tag{A48}$$
$$+\left(aG''\left(\varrho(x)\right)\frac{\partial}{\partial x}\varrho(x) - 2aEG'\left(\varrho(x)\right)\right)\cdot\frac{\partial}{\partial x}\bar{\varrho}_t(x)$$
$$+\left(\frac{a}{2}G'''\left(\varrho(x)\right)\left(\frac{\partial}{\partial x}\varrho(x)\right)^2 + \frac{a}{2}G''\left(\varrho(x)\right)\frac{\partial^2}{\partial x^2}\varrho(x) - 2aEG''\left(\varrho(x)\right)\frac{\partial}{\partial x}\varrho(x)\right)\cdot\bar{\varrho}_t(x)$$
$$+\mathcal{O}\left(\bar{\varrho}_t(x)\right)^2,$$

$$G'\left(\varrho(0)\right)\cdot\frac{\partial}{\partial x}\bar{\varrho}_t(0) = \left(4EG'\left(\varrho(0)\right) - G''\left(\varrho(0)\right)\frac{\partial}{\partial x}\varrho(0)\right)\cdot\bar{\varrho}_t(0) + \mathcal{O}\left(\bar{\varrho}_t(0)\right)^2, \tag{A49}$$

$$G'\left(\varrho(\ell)\right)\cdot\frac{\partial}{\partial x}\bar{\varrho}_t(\ell) = \left(4EG'\left(\varrho(\ell)\right) - G''\left(\varrho(\ell)\right)\frac{\partial}{\partial x}\varrho(\ell)\right)\cdot\bar{\varrho}_t(\ell) + \mathcal{O}\left(\bar{\varrho}_t(\ell)\right)^2. \tag{A50}$$

Neglecting error terms, the result is a linear equation, which may be solved numerically and used to fit the diffusivity a.

A6. Integrating the Continuum Equation

In section 3, we found an advection-diffusion equation describing the continuum evolution of the gradient process:

$$\frac{\partial}{\partial t}\varrho_t(x) \simeq \frac{a}{2}\frac{\partial^2}{\partial x^2}G\left(\varrho_t(x)\right) - 2aE\frac{\partial}{\partial x}G\left(\varrho_t(x)\right) \tag{A51}$$

with boundary conditions

$$\frac{\partial}{\partial x}G\left(\varrho_t(0)\right) = 4EG\left(\varrho_t(0)\right) \quad \text{and} \quad \frac{\partial}{\partial x}G(\varrho_t(1)) = 4EG(\varrho_t(1)). \tag{A52}$$

We can find the corresponding continuum equation for the hillslope profile by substituting $\varrho_t(x) = \frac{\partial}{\partial x}h_t(x)$, integrating with respect to x, and applying the boundary conditions

$$\frac{\partial}{\partial x}G\left(\frac{\partial}{\partial x}h_t(0)\right) = 4EG\left(\frac{\partial}{\partial x}h_t(0)\right) \quad \text{and} \quad \frac{\partial}{\partial x}G\left(\frac{\partial}{\partial x}h_t(1)\right) = 4EG\left(\frac{\partial}{\partial x}h_t(1)\right). \tag{A53}$$

We substitute and integrate as

$$\frac{\partial}{\partial t}\frac{\partial}{\partial x}h_t(x) = \frac{a}{2}\frac{\partial^2}{\partial x^2}G\left(\frac{\partial}{\partial x}h_t(x)\right) - 2aE\frac{\partial}{\partial x}G\left(\frac{\partial}{\partial x}h_t(x)\right), \tag{A54}$$

$$\int\frac{\partial}{\partial t}\frac{\partial}{\partial x}h_t(x)\mathrm{d}x = \frac{a}{2}\int\frac{\partial^2}{\partial x^2}G\left(\frac{\partial}{\partial x}h_t(x)\right)\mathrm{d}x - 2aE\int\frac{\partial}{\partial x}G\left(\frac{\partial}{\partial x}h_t(x)\right)\mathrm{d}x, \tag{A55}$$

$$\frac{\partial}{\partial t}h_t(x) = \frac{a}{2}\frac{\partial}{\partial x}G\left(\frac{\partial}{\partial x}h_t(x)\right) - 2aEG\left(\frac{\partial}{\partial x}h_t(x)\right) + C(t), \tag{A56}$$

where $C(t)$ is a function of t only. We can apply the boundary condition at $x = 0$, in terms of h_t, as

$$\frac{\partial}{\partial t}h_t(0) = \frac{a}{2}\frac{\partial}{\partial x}G\left(\frac{\partial}{\partial x}h_t(0)\right) - 2aEG\left(\frac{\partial}{\partial x}h_t(0)\right) + C(t) \tag{A57}$$

$$0 = \underbrace{\frac{a}{2}4EG\left(\frac{\partial}{\partial x}h_t(0)\right) - 2aEG\left(\frac{\partial}{\partial x}h_t(0)\right)}_{=0} + C(t). \tag{A58}$$

The argument for $x = 1$ is analogous, so we conclude that $C(t) = 0$ for all t and

$$\frac{\partial}{\partial t}h_t(x) = \frac{a}{2}\frac{\partial}{\partial x}G\left(\frac{\partial}{\partial x}h_t(x)\right) - 2aEG\left(\frac{\partial}{\partial x}h_t(x)\right). \tag{A59}$$

A7. Estimating Typical Distances Traveled by Particles

We begin with a disclaimer: This section is not part of the core scaling argument of section 3. This section is an example of how one might infer average distances traveled by units of hillslope; we cannot calculate this directly, as the *particles* of our model are units of gradient, not units of hillslope. To overcome this barrier, we settle for a mean-field argument. Rescaling is not involved, since one step of a grain is not imagined on scales comparable to the hillslope size. We therefore consider the slope $\varrho = \mathbb{E}\omega_i$ a constant parameter that changes as we look at different parts of the hill.

Consider, for the sake of argument, a medium flowing over the hillslope, which lifts, carries, and deposits units of hillslope, building up the heights h_i. We assume this medium flows at velocity $v(\varrho)$ (units of i/model time τ units) and that it tracks with particle deposition and removal, which happen at an average rate of $pe^{\theta(\varrho)}$. In other words, it takes an average time of $1/(pe^{\theta(\varrho)})$ for the flow to move between adjacent sites, and so we write

$$v(\varrho) = pe^{\theta(\varrho)}. \tag{A60}$$

Under our scaling, p is close to $1/2$, which we substitute.

We assume that a given grain spends an average time $\tau_0(\varrho)$ transported by the flow before depositing . The function τ_0 is an input of the model and might be constant or, perhaps more naturally, an increasing function of ϱ. This gives a deposition rate of $1/\tau_0(\varrho)$ and so the average distance traveled is

$$D(\varrho) = v(\varrho) \cdot \tau_0(\varrho) = \frac{1}{2} e^{\theta(\varrho)} \cdot \tau_0(\varrho). \tag{A61}$$

We assume that an average number $n(\varrho)$ of grains are carried by the flow per (microscopic) site (of the particle model). As over sufficiently long timescales the hillslope does not grow or vanish, the average flux Ψ of carried grains, $v(\varrho) \cdot n(\varrho)$ is conserved across the hillslope, from which we assert

$$n(\varrho) = \frac{\Psi}{v(\varrho)} = 2\Psi e^{-\theta(\varrho)}, \tag{A62}$$

a decreasing function of the slope ϱ. As each particle settles at rate $1/\tau_0(\varrho)$, the total rate at which particles are deposited at an individual site is

$$\frac{n(\varrho)}{\tau_0(\varrho)} = \frac{2\Psi e^{-\theta(\varrho)}}{\tau_0(\varrho)}. \tag{A63}$$

An essential feature of this model is to distinguish between a particle depositing on the hillslope and growth of a column in the gradient particle model. As the latter happens at an average rate of $\frac{1}{2}e^{\theta(\varrho)}$, every column-raising event of the gradient process is considered a deposition event for the hillslope as well with probability

$$\frac{4\Psi e^{-2\theta(\varrho)}}{\tau_0(\varrho)}, \tag{A64}$$

which must therefore be less than 1. Due to reversibility, we have the same rates and probabilities for entrainment.

A given particle takes part in a column growth event at average rate

$$\frac{e^{\theta(\varrho)}}{2n(\varrho)} = \frac{e^{2\theta(\varrho)}}{4\Psi}, \tag{A65}$$

an increasing function of slope. Multiplying this with the probability from the previous line recovers $1/\tau_0(\varrho)$ as the deposition rate.

To conclude, we have the following examples of average distance traveled:

$$D(\varrho) = \begin{cases} \frac{1}{2}\varrho\,\tau_0(\varrho) & \text{for linear rate,} \\ \frac{1}{2}\frac{\varrho}{1+\varrho}\,\tau_0(\varrho) & \text{for constant rate.} \end{cases} \tag{A66}$$

Acknowledgments
The authors acknowledge the generous support of the Marshall Scholarship (J. C.), Hungarian Scientific Research Fund (OTKA/NKFIH) grant K109684 (M. B.), and EPSRC standard grant EP/R0214491/1 (M. B.). No new data were used in producing this manuscript. The code for the model is freely available at https://github.com/csdms-contrib/1D-Particle-Based-Hillslope-Evolution-Model and listed in the Community Surface Dynamics Modeling System model repository at https://csdms.colorado.edu/wiki/Model:1D_Particle-Based_Hillslope_Evolution_Model. We thank the Editor, John M. Buffington, the Associate Editor, Jon Pelletier, and two anonymous reviewers, whose comprehensive comments and suggestions significantly improved the quality of the manuscript.

References

Ancey, C., Bohorquez, P., & Heyman, J. (2015). Stochastic interpretation of the advection-diffusion equation and its relevance to bed load transport. *Journal of Geophysical Research: Earth Surface*, *120*, 2529–2551. https://doi.org/10.1002/2014JF003421

Andrews, D., & Bucknam, R. C. (1987). Fitting degradation of shoreline scarps by a nonlinear diffusion model. *Journal of Geophysical Research*, *92*(B12), 12,857–12,867.

Bahadoran, C., Guiol, H., Ravishankar, K., & Saada, E. (2010). Strong hydrodynamic limit for attractive particle systems on Z. *Electronic Journal of Probability*, *15*, 1–43.

Balázs, M., & Bowen, R. (2016). Product blocking measures and a particle system proof of the Jacobi triple product. *Annales de l'Institut Henri Poincaré, Probabilités et Statistiques*, *54*, 514–528.

Balázs, M., & Seppäläinen, T. (2007). A convexity property of expectations under exponential weights. *arXiv preprint arXiv*, *0707*, 4273.

Booth, A. M., LaHusen, S. R., Duvall, A. R., & Montgomery, D. R. (2017). Holocene history of deep-seated landsliding in the North Fork Stillaguamish river valley from surface roughness analysis, radiocarbon dating, and numerical landscape evolution modeling. *Journal of Geophysical Research: Earth Surface*, *122*, 456–472. https://doi.org/10.1002/2016JF003934

Carson, M. A., & Kirkby, M. J. (1972). *Hillslope Form and Process*. New York: Cambridge University Press.

Culling, W. (1963). Soil creep and the development of hillside slopes. *The Journal of Geology*, *71*(2), 127–161.

Davies, J., Beven, K., Nyberg, L., & Rodhe, A. (2011). A discrete particle representation of hillslope hydrology: Hypothesis testing in reproducing a tracer experiment at Gårdsjön, Sweden. *Hydrological Processes*, *25*(23), 3602–3612.

DiBiase, R. A., Lamb, M. P., Ganti, V., & Booth, A. M. (2017). Slope, grain size, and roughness controls on dry sediment transport and storage on steep hillslopes. *Journal of Geophysical Research: Earth Surface*, *122*, 941–960. https://doi.org/10.1002/2016JF003970

Dietrich, W. E., Bellugi, D. G., Sklar, L. S., Stock, J. D., Heimsath, A. M., & Roering, J. J. (2003). Geomorphic transport laws for predicting landscape form and dynamics. *Prediction in Geomorphology*, *135*, 103–132.

Dunne, T., Malmon, D. V., & Mudd, S. M. (2010). A rain splash transport equation assimilating field and laboratory measurements. *Journal of Geophysical Research*, *115*, F01001. https://doi.org/10.1029/2009JF001302

Fathel, S. L., Furbish, D. J., & Schmeeckle, M. W. (2015). Experimental evidence of statistical ensemble behavior in bed load sediment transport. *Journal of Geophysical Research: Earth Surface*, *120*, 2298–2317. https://doi.org/10.1002/2015JF003552

Fernandes, N. F., & Dietrich, W. E. (1997). Hillslope evolution by diffusive processes: The timescale for equilibrium adjustments. *Water Resources Research*, *33*(6), 1307–1318.

Foufoula-Georgiou, E., Ganti, V., & Dietrich, W. (2010). A nonlocal theory of sediment transport on hillslopes. *Journal of Geophysical Research*, *115*, F00A16. https://doi.org/10.1029/2009JF001280

Furbish, D. J., Childs, E. M., Haff, P. K., & Schmeeckle, M. W. (2009). Rain splash of soil grains as a stochastic advection-dispersion process, with implications for desert plant-soil interactions and land-surface evolution. *Journal of Geophysical Research*, *114*, F00A03. https://doi.org/10.1029/2009JF001265

Furbish, D. J., & Haff, P. K. (2010). From divots to swales: Hillslope sediment transport across divers length scales. *Journal of Geophysical Research*, *115*, F03001. https://doi.org/10.1029/2009JF001576

Furbish, D. J., Haff, P. K., Dietrich, W. E., & Heimsath, A. M. (2009). Statistical description of slope-dependent soil transport and the diffusion-like coefficient. *Journal of Geophysical Research*, *114*, F00A05. https://doi.org/10.1029/2009JF001267

Furbish, D. J., & Roering, J. J. (2013). Sediment disentrainment and the concept of local versus nonlocal transport on hillslopes. *Journal of Geophysical Research: Earth Surface*, *118*, 937–952. https://doi.org/10.1002/jgrf.20071

Gabet, E. J. (2000). Gopher bioturbation: Field evidence for non-linear hillslope diffusion. *Earth Surface Processes and Landforms*, *25*(13), 1419–1428.

Gabet, E. J., & Mendoza, M. K. (2012). Particle transport over rough hillslope surfaces by dry ravel: Experiments and simulations with implications for nonlocal sediment flux. *Journal of Geophysical Research*, *117*, F01019. https://doi.org/10.1029/2011JF002229

Gabet, E. J., Reichman, O., & Seabloom, E. W. (2003). The effects of bioturbation on soil processes and sediment transport. *Annual Review of Earth and Planetary Sciences*, *31*(1), 249–273.

Ganti, V., Passalacqua, P., & Foufoula-Georgiou, E. (2012). A sub-grid scale closure for nonlinear hillslope sediment transport models. *Journal of Geophysical Research*, *117*, F02012. https://doi.org/10.1029/2011JF002181

Habersack, H. (2001). Radio-tracking gravel particles in a large braided river in New Zealand: A field test of the stochastic theory of bed load transport proposed by Einstein. *Hydrological Processes*, *15*(3), 377–391.

Harvey, A. M. (1994). Influence of slope/stream coupling on process interactions on eroding gully slopes: Howgill Fells, northwest England. In M. J. Kirkby (Ed.), *Process Models and Theoretical Geomorphology* (pp. 247–270). Chichester: Wiley.

Kessler, M., & Werner, B. (2003). Self-organization of sorted patterned ground. *Science*, *299*(5605), 380–383.

Kipnis, C., & Landim, C. (1999). *Scaling Limits of Interacting Particle Systems*. Berlin: Springer.

Kirkby, M. J. (1971). Hillslope process-response models based on the continuity equation. *Special Publication Institute of British Geographers*, *3*, 15–30.

Kirkby, M., & Statham, I. (1975). Surface stone movement and scree formation. *The Journal of Geology*, *83*(3), 349–362.

McNamara, J. P., & Borden, C. (2004). Observations on the movement of coarse gravel using implanted motion-sensing radio transmitters. *Hydrological Processes*, *18*(10), 1871–1884.

Michaelides, K., & Martin, G. J. (2012). Sediment transport by runoff on debris-mantled dryland hillslopes. *Journal of Geophysical Research*, *117*, F03014. https://doi.org/10.1029/2012JF002415

Michaelides, K., & Singer, M. B. (2014). Impact of coarse sediment supply from hillslopes to the channel in runoff-dominated, dryland fluvial systems. *Journal of Geophysical Research: Earth Surface*, *119*, 1205–1221. https://doi.org/10.1002/2013JF002959

Mudd, S. M., & Furbish, D. J. (2004). Influence of chemical denudation on hillslope morphology. *Journal of Geophysical Research*, *109*, F02001. https://doi.org/10.1029/2003JF000087

Olla, S., Varadhan, S., & Yau, H. (1993). Hydrodynamical limit for a Hamiltonian system with weak noise. *Communications in Mathematical Physics*, *155*(3), 523–560.

Roering, J. J. (2004). Soil creep and convex-upward velocity profiles: Theoretical and experimental investigation of disturbance-driven sediment transport on hillslopes. *Earth Surface Processes and Landforms*, *29*(13), 1597–1612.

Roering, J. J., Kirchner, J. W., & Dietrich, W. E. (1999). Evidence for nonlinear, diffusive sediment transport on hillslopes and implications for landscape morphology. *Water Resources Research*, *35*(3), 853–870.

Roering, J. J., Kirchner, J. W., & Dietrich, W. E. (2001). Hillslope evolution by nonlinear, slope-dependent transport: Steady state morphology and equilibrium adjustment timescales. *Journal of Geophysical Research*, *106*(B8), 16,499–16,513.

Roering, J. J., Perron, J. T., & Kirchner, J. W. (2007). Functional relationships between denudation and hillslope form and relief. *Earth and Planetary Science Letters*, *264*(1-2), 245–258.

Roseberry, J. C., Schmeeckle, M. W., & Furbish, D. J. (2012). A probabilistic description of the bed load sediment flux: 2. particle activity and motions. *Journal of Geophysical Research*, *117*, F03032. https://doi.org/10.1029/2012JF002353

Tucker, G. E., & Bradley, D. N. (2010). Trouble with diffusion: Reassessing hillslope erosion laws with a particle-based model. *Journal of Geophysical Research*, *115*, F00A10. https://doi.org/10.1029/2009JF001264

Tucker, G. E., & Hancock, G. R. (2010). Modelling landscape evolution. *Earth Surface Processes and Landforms*, *35*(1), 28–50.